PRD Draft Version 0.3
February 12, 2007

Search for Standard Model Higgs Boson Production in Association with W Boson at CDF

A. Abulencia,[23] J. Adelman,[13] T. Affolder,[10] T. Akimoto,[55] M.G. Albrow,[16] D. Ambrose,[16] S. Amerio,[43] D. Amidei,[34] A. Anastassov,[52] K. Anikeev,[16] A. Annovi,[18] J. Antos,[1] M. Aoki,[55] G. Apollinari,[16] J.-F. Arguin,[33] T. Arisawa,[57] A. Artikov,[14] W. Ashmanskas,[16] A. Attal,[8] F. Azfar,[42] P. Azzi-Bacchetta,[43] P. Azzurri,[46] N. Bacchetta,[43] W. Badgett,[16] A. Barbaro-Galtieri,[28] V.E. Barnes,[48] B.A. Barnett,[24] S. Baroiant,[7] V. Bartsch,[30] G. Bauer,[32] F. Bedeschi,[46] S. Behari,[24] S. Belforte,[54] G. Bellettini,[46] J. Bellinger,[59] A. Belloni,[32] D. Benjamin,[15] A. Beretvas,[16] J. Beringer,[28] T. Berry,[29] A. Bhatti,[50] M. Binkley,[16] D. Bisello,[43] R.E. Blair,[2] C. Blocker,[6] B. Blumenfeld,[24] A. Bocci,[15] A. Bodek,[49] V. Boisvert,[49] G. Bolla,[48] A. Bolshov,[32] D. Bortoletto,[48] J. Boudreau,[47] A. Boveia,[10] B. Brau,[10] L. Brigliadori,[5] C. Bromberg,[35] E. Brubaker,[13] J. Budagov,[14] H.S. Budd,[49] S. Budd,[23] S. Budroni,[46] K. Burkett,[16] G. Busetto,[43] P. Bussey,[20] K. L. Byrum,[2] S. Cabrera,[15] M. Campanelli,[19] M. Campbell,[34] F. Canelli,[16] A. Canepa,[48] S. Carillo,[17] D. Carlsmith,[59] R. Carosi,[46] M. Casarsa,[54] A. Castro,[5] P. Catastini,[46] D. Cauz,[54] M. Cavalli-Sforza,[3] A. Cerri,[28] L. Cerrito,[42] S.H. Chang,[27] Y.C. Chen,[1] M. Chertok,[7] G. Chiarelli,[46] G. Chlachidze,[14] F. Chlebana,[16] I. Cho,[27] K. Cho,[27] D. Chokheli,[14] J.P. Chou,[21] G. Choudalakis,[32] S.H. Chuang,[59] K. Chung,[12] W.H. Chung,[59] Y.S. Chung,[49] M. Ciljak,[46] C.I. Ciobanu,[23] M.A. Ciocci,[46] A. Clark,[19] D. Clark,[6] M. Coca,[15] G. Compostella,[43] M.E. Convery,[50] J. Conway,[7] B. Cooper,[35] K. Copic,[34] M. Cordelli,[18] G. Cortiana,[43] F. Crescioli,[46] C. Cuenca Almenar,[7] J. Cuevas,[11] R. Culbertson,[16] J.C. Cully,[34] D. Cyr,[59] S. DaRonco,[43] S. D'Auria,[20] T. Davies,[20] M. D'Onofrio,[3] D. Dagenhart,[6] P. de Barbaro,[49] S. De Cecco,[51] A. Deisher,[28] G. De Lentdecker,[49] M. Dell'Orso,[46] F. Delli Paoli,[43] L. Demortier,[50] J. Deng,[15] M. Deninno,[5] D. De Pedis,[51] P.F. Derwent,[16] G.P. Di Giovanni,[44] C. Dionisi,[51] B. Di Ruzza,[54] J.R. Dittmann,[4] P. DiTuro,[52] C. Dörr,[25] S. Donati,[46] M. Donega,[19] P. Dong,[8] J. Donini,[43] T. Dorigo,[43] S. Dube,[52] J. Efron,[39] R. Erbacher,[7] D. Errede,[23] S. Errede,[23] R. Eusebi,[16] H.C. Fang,[28] S. Farrington,[29] I. Fedorko,[46] W.T. Fedorko,[13] R.G. Feild,[60] M. Feindt,[25] J.P. Fernandez,[31] R. Field,[17] G. Flanagan,[48] A. Foland,[21] S. Forrester,[7] G.W. Foster,[16] M. Franklin,[21] J.C. Freeman,[28] I. Furic,[13] M. Gallinaro,[50] J. Galyardt,[12] J.E. Garcia,[46] F. Garberson,[10] A.F. Garfinkel,[48] C. Gay,[60] H. Gerberich,[23] D. Gerdes,[34] S. Giagu,[51] P. Giannetti,[46] A. Gibson,[28] K. Gibson,[47] J.L. Gimmell,[49] C. Ginsburg,[16] N. Giokaris,[14] M. Giordani,[54] P. Giromini,[18] M. Giunta,[46] G. Giurgiu,[12] V. Glagolev,[14] D. Glenzinski,[16] M. Gold,[37] N. Goldschmidt,[17] J. Goldstein,[42] G. Gomez,[11] G. Gomez-Ceballos,[11] M. Goncharov,[53] O. González,[31] I. Gorelov,[37] A.T. Goshaw,[15] K. Goulianos,[50] A. Gresele,[43] M. Griffiths,[29] S. Grinstein,[21] C. Grosso-Pilcher,[13] R.C. Group,[17] U. Grundler,[23] J. Guimaraes da Costa,[21] Z. Gunay-Unalan,[35] C. Haber,[28] K. Hahn,[32] S.R. Hahn,[16] E. Halkiadakis,[52] A. Hamilton,[33] B.-Y. Han,[49] J.Y. Han,[49] R. Handler,[59] F. Happacher,[18] K. Hara,[55] M. Hare,[56] S. Harper,[42] R.F. Harr,[58] R.M. Harris,[16] M. Hartz,[47] K. Hatakeyama,[50] J. Hauser,[8] A. Heijboer,[45] B. Heinemann,[29] J. Heinrich,[45] C. Henderson,[32] M. Herndon,[59] J. Heuser,[25] D. Hidas,[15] C.S. Hill,[10] D. Hirschbuehl,[25] A. Hocker,[16] A. Holloway,[21] S. Hou,[1] M. Houlden,[29] S.-C. Hsu,[9] B.T. Huffman,[42] R.E. Hughes,[39] U. Husemann,[60] J. Huston,[35] J. Incandela,[10] G. Introzzi,[46] M. Iori,[51] Y. Ishizawa,[55] A. Ivanov,[7] B. Iyutin,[32] E. James,[16] D. Jang,[52] B. Jayatilaka,[34] D. Jeans,[51] H. Jensen,[16] E.J. Jeon,[27] S. Jindariani,[17] M. Jones,[48] K.K. Joo,[27] S.Y. Jun,[12] J.E. Jung,[27] T.R. Junk,[23] T. Kamon,[53] P.E. Karchin,[58] Y. Kato,[41] Y. Kemp,[25] R. Kephart,[16] U. Kerzel,[25] V. Khotilovich,[53] B. Kilminster,[39] D.H. Kim,[27] H.S. Kim,[27] J.E. Kim,[27] M.J. Kim,[12] S.B. Kim,[27] S.H. Kim,[55] Y.K. Kim,[13] N. Kimura,[55] L. Kirsch,[6] S. Klimenko,[17] M. Klute,[32] B. Knuteson,[32] B.R. Ko,[15] K. Kondo,[57] D.J. Kong,[27] J. Konigsberg,[17] A. Korytov,[17] A.V. Kotwal,[15] A. Kovalev,[45] A.C. Kraan,[45] J. Kraus,[23] I. Kravchenko,[32] M. Kreps,[25] J. Kroll,[45] N. Krumnack,[4] M. Kruse,[15] V. Krutelyov,[10] T. Kubo,[55] S. E. Kuhlmann,[2] T. Kuhr,[25] Y. Kusakabe,[57] S. Kwang,[13] A.T. Laasanen,[48] S. Lai,[33] S. Lami,[46] S. Lammel,[16] M. Lancaster,[30] R.L. Lander,[7] K. Lannon,[39] A. Lath,[52] G. Latino,[46] I. Lazzizzera,[43] T. LeCompte,[2] J. Lee,[49] J. Lee,[27] Y.J. Lee,[27] S.W. Lee,[53] R. Lefèvre,[3] N. Leonardo,[32] S. Leone,[46] S. Levy,[13] J.D. Lewis,[16] C. Lin,[60] C.S. Lin,[16] M. Lindgren,[16] E. Lipeles,[9] A. Lister,[7] D.O. Litvintsev,[16] T. Liu,[16] N.S. Lockyer,[45] A. Loginov,[36] M. Loreti,[43] P. Loverre,[51] R.-S. Lu,[1] D. Lucchesi,[43] P. Lujan,[28] P. Lukens,[16] G. Lungu,[17] L. Lyons,[42] J. Lys,[28] R. Lysak,[1] E. Lytken,[48] P. Mack,[25] D. MacQueen,[33] R. Madrak,[16] K. Maeshima,[16] K. Makhoul,[32] T. Maki,[22] P. Maksimovic,[24] S. Malde,[42] G. Manca,[29] F. Margaroli,[5] R. Marginean,[16] C. Marino,[25] C.P. Marino,[23] A. Martin,[60] M. Martin,[20] V. Martin,[20] M. Martínez,[3] T. Maruyama,[55] P. Mastrandrea,[51] T. Masubuchi,[55] H. Matsunaga,[55] M.E. Mattson,[58] R. Mazini,[33] P. Mazzanti,[5] K.S. McFarland,[49] P. McIntyre,[53] R. McNulty,[29] A. Mehta,[29] P. Mehtala,[22] S. Menzemer,[11] A. Menzione,[46] P. Merkel,[48] C. Mesropian,[50] A. Messina,[35] T. Miao,[16] N. Miladinovic,[6] J. Miles,[32] R. Miller,[35] C. Mills,[10] M. Milnik,[25] A. Mitra,[1] G. Mitselmakher,[17] A. Miyamoto,[26]

S. Moed,[19] N. Moggi,[5] B. Mohr,[8] R. Moore,[16] M. Morello,[46] P. Movilla Fernandez,[28] J. Mülmenstädt,[28] A. Mukherjee,[16] Th. Muller,[25] R. Mumford,[24] P. Murat,[16] J. Nachtman,[16] A. Nagano,[55] J. Naganoma,[57] I. Nakano,[40] A. Napier,[56] V. Necula,[17] C. Neu,[45] M.S. Neubauer,[9] J. Nielsen,[28] T. Nigmanov,[47] L. Nodulman,[2] O. Norniella,[3] E. Nurse,[30] S.H. Oh,[15] Y.D. Oh,[27] I. Oksuzian,[17] T. Okusawa,[41] R. Oldeman,[29] R. Orava,[22] K. Osterberg,[22] C. Pagliarone,[46] E. Palencia,[11] V. Papadimitriou,[16] A.A. Paramonov,[13] B. Parks,[39] S. Pashapour,[33] J. Patrick,[16] G. Pauletta,[54] M. Paulini,[12] C. Paus,[32] D.E. Pellett,[7] A. Penzo,[54] T.J. Phillips,[15] G. Piacentino,[46] J. Piedra,[44] L. Pinera,[17] K. Pitts,[23] C. Plager,[8] L. Pondrom,[59] X. Portell,[3] O. Poukhov,[14] N. Pounder,[42] F. Prakoshyn,[14] A. Pronko,[16] J. Proudfoot,[2] F. Ptohos,[18] G. Punzi,[46] J. Pursley,[24] J. Rademacker,[42] A. Rahaman,[47] N. Ranjan,[48] S. Rappoccio,[21] B. Reisert,[16] V. Rekovic,[37] P. Renton,[42] M. Rescigno,[51] S. Richter,[25] F. Rimondi,[5] L. Ristori,[46] A. Robson,[20] T. Rodrigo,[11] E. Rogers,[23] S. Rolli,[56] R. Roser,[16] M. Rossi,[54] R. Rossin,[17] A. Ruiz,[11] J. Russ,[12] V. Rusu,[13] H. Saarikko,[22] S. Sabik,[33] A. Safonov,[53] W.K. Sakumoto,[49] G. Salamanna,[51] O. Saltó,[3] D. Saltzberg,[8] C. Sánchez,[3] L. Santi,[54] S. Sarkar,[51] L. Sartori,[46] K. Sato,[16] P. Savard,[33] A. Savoy-Navarro,[44] T. Scheidle,[25] P. Schlabach,[16] E.E. Schmidt,[16] M.P. Schmidt,[60] M. Schmitt,[38] T. Schwarz,[7] L. Scodellaro,[11] A.L. Scott,[10] A. Scribano,[46] F. Scuri,[46] A. Sedov,[48] S. Seidel,[37] Y. Seiya,[41] A. Semenov,[14] L. Sexton-Kennedy,[16] A. Sfyrla,[19] M.D. Shapiro,[28] T. Shears,[29] P.F. Shepard,[47] D. Sherman,[21] M. Shimojima,[55] M. Shochet,[13] Y. Shon,[59] I. Shreyber,[36] A. Sidoti,[46] P. Sinervo,[33] A. Sisakyan,[14] J. Sjolin,[42] A.J. Slaughter,[16] J. Slaunwhite,[39] K. Sliwa,[56] J.R. Smith,[7] F.D. Snider,[16] R. Snihur,[33] M. Soderberg,[34] A. Soha,[7] S. Somalwar,[52] V. Sorin,[35] J. Spalding,[16] F. Spinella,[46] T. Spreitzer,[33] P. Squillacioti,[46] M. Stanitzki,[60] A. Staveris-Polykalas,[46] R. St. Denis,[20] B. Stelzer,[8] O. Stelzer-Chilton,[42] D. Stentz,[38] J. Strologas,[37] D. Stuart,[10] J.S. Suh,[27] A. Sukhanov,[17] H. Sun,[56] T. Suzuki,[55] A. Taffard,[23] R. Takashima,[40] Y. Takeuchi,[55] K. Takikawa,[55] M. Tanaka,[2] R. Tanaka,[40] M. Tecchio,[34] P.K. Teng,[1] K. Terashi,[50] J. Thom,[16] A.S. Thompson,[20] E. Thomson,[45] P. Tipton,[60] V. Tiwari,[12] S. Tkaczyk,[16] D. Toback,[53] S. Tokar,[14] K. Tollefson,[35] T. Tomura,[55] D. Tonelli,[46] S. Torre,[18] D. Torretta,[16] S. Tourneur,[44] W. Trischuk,[33] R. Tsuchiya,[57] S. Tsuno,[40] N. Turini,[46] F. Ukegawa,[55] T. Unverhau,[20] S. Uozumi,[55] D. Usynin,[45] S. Vallecorsa,[19] N. van Remortel,[22] A. Varganov,[34] E. Vataga,[37] F. Vázquez,[17] G. Velev,[16] G. Veramendi,[23] V. Veszpremi,[48] R. Vidal,[16] I. Vila,[11] R. Vilar,[11] T. Vine,[30] I. Vollrath,[33] I. Volobouev,[28] G. Volpi,[46] F. Würthwein,[9] P. Wagner,[53] R.G. Wagner,[2] R.L. Wagner,[16] J. Wagner,[25] W. Wagner,[25] R. Wallny,[8] S.M. Wang,[1] A. Warburton,[33] S. Waschke,[20] D. Waters,[30] W.C. Wester III,[16] B. Whitehouse,[56] D. Whiteson,[45] A.B. Wicklund,[2] E. Wicklund,[16] G. Williams,[33] H.H. Williams,[45] P. Wilson,[16] B.L. Winer,[39] P. Wittich,[16] S. Wolbers,[16] C. Wolfe,[13] T. Wright,[34] X. Wu,[19] S.M. Wynne,[29] A. Yagil,[16] K. Yamamoto,[41] J. Yamaoka,[52] T. Yamashita,[40] C. Yang,[60] U.K. Yang,[13] Y.C. Yang,[27] W.M. Yao,[28] G.P. Yeh,[16] J. Yoh,[16] K. Yorita,[13] T. Yoshida,[41] G.B. Yu,[49] I. Yu,[27] S.S. Yu,[16] J.C. Yun,[16] L. Zanello,[51] A. Zanetti,[54] I. Zaw,[21] X. Zhang,[23] J. Zhou,[52] and S. Zucchelli[5]

(CDF Collaboration)

[1]*Institute of Physics, Academia Sinica, Taipei, Taiwan 11529, Republic of China*
[2]*Argonne National Laboratory, Argonne, Illinois 60439*
[3]*Institut de Fisica d'Altes Energies, Universitat Autonoma de Barcelona, E-08193, Bellaterra (Barcelona), Spain*
[4]*Baylor University, Waco, Texas 76798*
[5]*Istituto Nazionale di Fisica Nucleare, University of Bologna, I-40127 Bologna, Italy*
[6]*Brandeis University, Waltham, Massachusetts 02254*
[7]*University of California, Davis, Davis, California 95616*
[8]*University of California, Los Angeles, Los Angeles, California 90024*
[9]*University of California, San Diego, La Jolla, California 92093*
[10]*University of California, Santa Barbara, Santa Barbara, California 93106*
[11]*Instituto de Fisica de Cantabria, CSIC-University of Cantabria, 39005 Santander, Spain*
[12]*Carnegie Mellon University, Pittsburgh, PA 15213*
[13]*Enrico Fermi Institute, University of Chicago, Chicago, Illinois 60637*
[14]*Joint Institute for Nuclear Research, RU-141980 Dubna, Russia*
[15]*Duke University, Durham, North Carolina 27708*
[16]*Fermi National Accelerator Laboratory, Batavia, Illinois 60510*
[17]*University of Florida, Gainesville, Florida 32611*
[18]*Laboratori Nazionali di Frascati, Istituto Nazionale di Fisica Nucleare, I-00044 Frascati, Italy*
[19]*University of Geneva, CH-1211 Geneva 4, Switzerland*
[20]*Glasgow University, Glasgow G12 8QQ, United Kingdom*
[21]*Harvard University, Cambridge, Massachusetts 02138*
[22]*Division of High Energy Physics, Department of Physics, University of Helsinki and Helsinki Institute of Physics, FIN-00014, Helsinki, Finland*
[23]*University of Illinois, Urbana, Illinois 61801*
[24]*The Johns Hopkins University, Baltimore, Maryland 21218*

[25]Institut für Experimentelle Kernphysik, Universität Karlsruhe, 76128 Karlsruhe, Germany
[26]High Energy Accelerator Research Organization (KEK), Tsukuba, Ibaraki 305, Japan
[27]Center for High Energy Physics: Kyungpook National University,
Taegu 702-701, Korea; Seoul National University, Seoul 151-742,
Korea; and SungKyunKwan University, Suwon 440-746, Korea
[28]Ernest Orlando Lawrence Berkeley National Laboratory, Berkeley, California 94720
[29]University of Liverpool, Liverpool L69 7ZE, United Kingdom
[30]University College London, London WC1E 6BT, United Kingdom
[31]Centro de Investigaciones Energeticas Medioambientales y Tecnologicas, E-28040 Madrid, Spain
[32]Massachusetts Institute of Technology, Cambridge, Massachusetts 02139
[33]Institute of Particle Physics: McGill University, Montréal,
Canada H3A 2T8; and University of Toronto, Toronto, Canada M5S 1A7
[34]University of Michigan, Ann Arbor, Michigan 48109
[35]Michigan State University, East Lansing, Michigan 48824
[36]Institution for Theoretical and Experimental Physics, ITEP, Moscow 117259, Russia
[37]University of New Mexico, Albuquerque, New Mexico 87131
[38]Northwestern University, Evanston, Illinois 60208
[39]The Ohio State University, Columbus, Ohio 43210
[40]Okayama University, Okayama 700-8530, Japan
[41]Osaka City University, Osaka 588, Japan
[42]University of Oxford, Oxford OX1 3RH, United Kingdom
[43]University of Padova, Istituto Nazionale di Fisica Nucleare,
Sezione di Padova-Trento, I-35131 Padova, Italy
[44]LPNHE, Universite Pierre et Marie Curie/IN2P3-CNRS, UMR7585, Paris, F-75252 France
[45]University of Pennsylvania, Philadelphia, Pennsylvania 19104
[46]Istituto Nazionale di Fisica Nucleare Pisa, Universities of Pisa,
Siena and Scuola Normale Superiore, I-56127 Pisa, Italy
[47]University of Pittsburgh, Pittsburgh, Pennsylvania 15260
[48]Purdue University, West Lafayette, Indiana 47907
[49]University of Rochester, Rochester, New York 14627
[50]The Rockefeller University, New York, New York 10021
[51]Istituto Nazionale di Fisica Nucleare, Sezione di Roma 1,
University of Rome "La Sapienza," I-00185 Roma, Italy
[52]Rutgers University, Piscataway, New Jersey 08855
[53]Texas A&M University, College Station, Texas 77843
[54]Istituto Nazionale di Fisica Nucleare, University of Trieste/ Udine, Italy
[55]University of Tsukuba, Tsukuba, Ibaraki 305, Japan
[56]Tufts University, Medford, Massachusetts 02155
[57]Waseda University, Tokyo 169, Japan
[58]Wayne State University, Detroit, Michigan 48201
[59]University of Wisconsin, Madison, Wisconsin 53706
[60]Yale University, New Haven, Connecticut 06520

We present a search for Standard Model Higgs boson production in association with W boson ($p\bar{p} \to W^{\pm}H \to \ell\nu b\bar{b}$) in proton-antiproton collisions at a center of mass energy of 1.96 TeV. The search employs data collected by the CDF II detector which correspond to an integrated luminosity of approximately 1 fb^{-1}. We select events with a single lepton($e^{\pm}/\mu^{\pm}$), missing transverse energy and two jets. Jets corresponding to bottom quarks are identified with a secondary vertex tagging method and a neural network filter technique. The observed number of events and dijet mass distributions are consistent with the standard model background expectations, and we set a 95% confidence level upper limit on the production cross section times branching ratio of 3.9 to 1.3 pb for Higgs boson mass 110 to 150GeV/c^2.

PACS numbers:

I. INTRODUCTION

Standard electroweak theory predicts a single fundamental scalar field, the Higgs field, which spontaneously breaks the electroweak gauge symmetry. However, the Higgs boson, the quantized Higgs field, has not been observed experimentally. The current constraints on the Higgs boson mass ($114.4 < m_H < 199$ GeV/c^2 at 95% confidence level(C.L.)) come from direct Higgs boson searches at LEP2 experiments[1] and electroweak global fits[2]. These results imply that the Higgs boson is relatively light.

The Next to Leading Order(NLO) Higgs boson production cross section at the Tevatron[3] is shown in Fig.1. The gluon fusion Higgs production has about 10 times

larger cross section than WH process, and the cross section of WH process is about twice as much as ZH production. The Higgs boson decay branching ratio[4] is

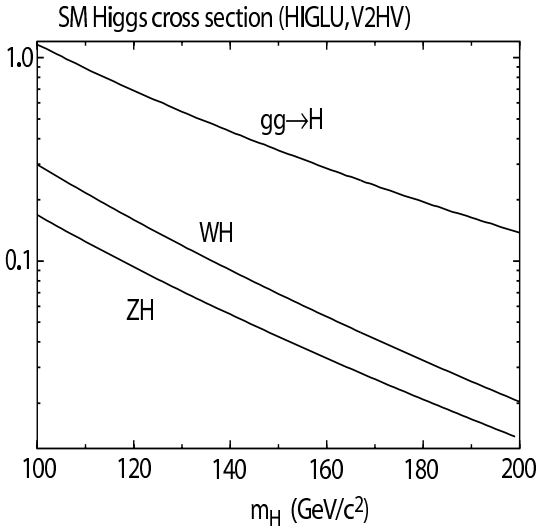

FIG. 1: The NLO Higgs boson production cross section for $gg \to H$, $q\bar{q}' \to WH$, and $q\bar{q} \to ZH$ processes as a function of Higgs boson mass at the Tevatron ($p\bar{p}$ collision, $\sqrt{s} = 1.96$ TeV).

shown in Fig.2. Higgs boson decay is dominated by the $H \to b\bar{b}$ mode for m_H <135 GeV/c^2, and $H \to W^+W^-$ mode for m_H >135 GeV/c^2. In general, QCD multi-jet processes have far larger cross sections than that of Higgs boson production. This seems to imply that Higgs boson searches in the processes $gg \to H \to b\bar{b}$, $WH \to q\bar{q}'b\bar{b}$, and $ZH \to q\bar{q}b\bar{b}$ are not expected to have good sensitivities. However, the requirement of the leptonic decay of the associated weak boson reduces the huge QCD background rate. As a result, $WH \to \ell\nu b\bar{b}$ is considered to be one of the most sensitive processes for low mass Higgs boson searches ($m_H < 135$ GeV/c^2)[33]. Searches for $WH \to \ell\nu b\bar{b}$ in Tevatron RUN II have been reported previously by CDF(319 pb^{-1})[5] and DØ(174 pb^{-1})[6]. The previous analysis at CDF used the secondary vertex (SECVTX) b-tagging algorithm to distinguish jets originating from b quarks from other light flavor jets. Events with a lepton ($e^{\pm}/\mu^{\pm}$), missing transverse E_T ($\not\!\!E_T$) and two jets, at least one of which is identified as b jet, are selected. The number of events and dijet mass distributions are consistent with the standard model background prediction, and the Higgs boson production is constrained as follows.

$$\sigma(p\bar{p} \to WH) \cdot Br(H \to b\bar{b}) < 10 - 2.8 \text{ (pb)}$$

for $m_H = 110 - 150$ GeV/c^{2}at 95% C.L..

However, about 50% of the jets tagged by the SECVTX tagging algorithm are contaminated by falsely tagged jets originating from light flavor or charm quarks due to the finite resolution of track measurements or the

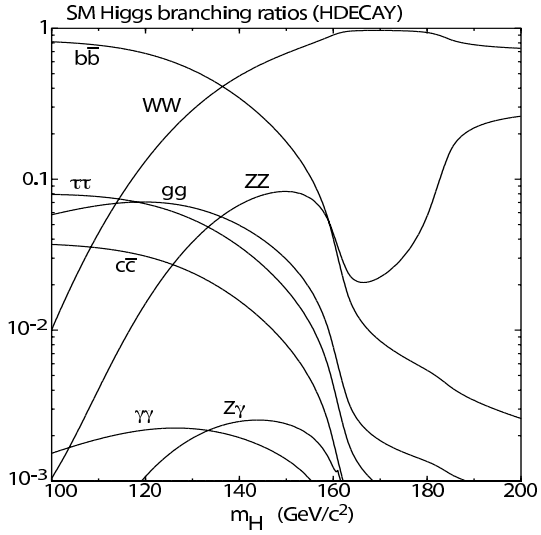

FIG. 2: The branching ratio for each Higgs boson decay mode as a function of Higgs boson mass.

long lifetime of D mesons. To reduce the contamination, we introduce a b-tagging neural network using jet variables in addition to SECVTX tagging. In this paper, we present a search for $WH \to \ell\nu b\bar{b}$ process at CDF using about 1 fb^{-1} of data, organized as follows. The next section starts from event detection and reconstruction with a review of the CDF II detector relevant to this analysis. In section III, the b-tagging algorithm with SECVTX and neural network are discussed in detail. Section IV explains the event selection criteria. Estimation of the standard model background is explained in section V for respective background sources. In section VI, signal acceptance and systematic uncertainties are estimated, and final likelihood results for the Higgs search are presented. Finally, conclusions are given in section VII.

II. EVENT DETECTION AND RECONSTRUCTION

III. b-TAGGING

In this section, the b-tagging method is discussed. Physics processes with jets of final state observable particles have huge contributions from QCD light flavor jet background, and searches in this final state face a sensitivity challenge. Important physics processes that include standard model Higgs boson or top quarks are expected to have a large branching fraction to bottom quarks in the final state. Therefore it is critical to identify correctly jets from b quarks as b jets. This helps remove most of the enormous QCD light flavor jet rate. Three ways of b-jets identification techniques have been developed and used in analyses in CDF by utilizing the properties of the b quark. "Soft Lepton b-Tagging (SLT)"

uses the lepton kinematics from the semileptonic decay of B-meson, but the semileptonic branching ratio is only about 10% [7, 8]. "Jet Probability b-tagging (JetProb)" uses the impact parameters of the tracks in the jets to determine the probability for the tracks to have come from the primary vertex. Then, jets with tracks having some probability not to have come from the primary vertex are assigned as b-jets[9, 10]. "Secondary Vertex b-tagging(SECVTX)" used in this search utilizes the property that b quark show a displaced secondary vertex. However, the SECVTX b-tagging still has significant contamination from false tags and the misidentification of c quarks as b-jets. This search introduces for the first time a multivariate neural network (NN) technique intended to overcome this difficulty and improve SECVTX tagging purity.

A. Displaced Secondary Vertex b-Tagging

The b-quark has a relatively long lifetime of 1.5×10^{-12} s and a large mass of approximately 5GeV/c^2. This means that the B hadrons formed during the hadronization of the initial b-quark can travel a significant distance before decaying into a collection of lighter hadrons. The spot where the decay happens can be reconstructed in the micro-strip silicon detector by identifying tracks which form a secondary vertex significantly displaced from the primary $p\bar{p}$ interaction point (primary vertex).

SECVTX b-tagging is performed for each jet in the event, using only the tracks which are within η-ϕ distance of $\Delta R = 0.4$ of the jet. Poorly reconstructed tracks are not used for SECVTX finding.[34] To find secondary vertices, at least two good quality tracks are necessary. Displaced tracks in jets, which are determined by impact parameter significance defined as $|d_0/\sigma_{d_0}|$ where d_0 and σ_{d_0} are impact parameter and total uncertainty from tracking and beam position measurements, are used for the SECVTX reconstruction. Secondary vertices are reconstructed by a two-pass approach.

Pass 1: At least three tracks are required to pass loose selection criteria ($p_T > 0.5$ GeV/c, $|d_0/\sigma_{d_0}| > 2.0$), and a secondary vertex is fit from the selected tracks. One of the tracks used in the reconstruction is required to have $p_T > 1.0$ GeV/c^2.

Pass 2: Exactly two tracks are required to pass tight selection criteria ($p_T > 1.0$ GeV/c, $|d_0/\sigma_{d_0}| > 3.5$ One of the tracks must have $p_T > 1.5$ GeV/c). Then reconstruct secondary vertex from the two tracks.

The algorithm reaches pass 2 only when pass 1 fails. If either pass is successful, the transverse distance L_{xy} from the primary vertex of the event is calculated along with the associated uncertainty on L_{xy}. This uncertainty $\sigma_{L_{xy}}$ includes the uncertainty on the primary vertex position. Finally jets are tagged positively or negatively depending on the L_{xy} significance $L_{xy}/\sigma_{L_{xy}}$ [11]:

$$L_{xy}/\sigma_{L_{xy}} \geq 7.5 \quad \text{(positive tag)} \tag{1}$$
$$L_{xy}/\sigma_{L_{xy}} \leq -7.5 \quad \text{(negative tag)} \tag{2}$$

The sign of L_{xy} indicates the position of the secondary

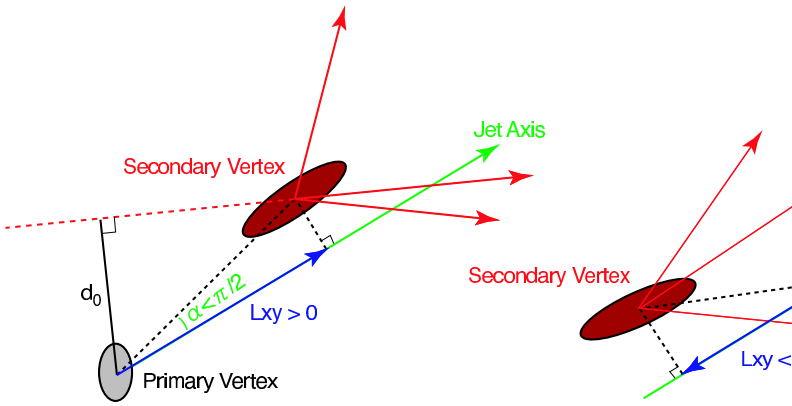

FIG. 3: Cartoon showing true reconstructed secondary vertex ($L_{xy} > 0$, left) and fake one ($L_{xy} < 0$, right).

vertex with respect to the primary vertex along the direction of the jet as illustrated in Fig.3. If the angle between the jet direction and the vector pointing from primary vertex to the secondary vertex is less than $\pi/2$, L_{xy} is positively defined. Otherwise, it becomes negative. If L_{xy} is positive, the secondary vertex points towards the direction of the jet. This is consistent with a B hadron traveling from the primary vertex in the direction of the jet. Of course, positive L_{xy} is preferred in true B hadron decays. For negative L_{xy} the secondary vertex points away from the jet; this usually happens as a result of mis-measured tracks. Jets tagged with a negative L_{xy} are labeled mis-tagged jets. Additionally, in order to reject secondary vertices due to material interaction, the algorithm requires secondary vertices satisfy the following requirements:

- **Pass 2** vertices found between 1.2 and 2.5 cm from the center of SVX[35] are vetoed.
- All vertices having radius greater than 2.5 cm with respect to the center of the SVX are vetoed.

The negative tags are useful for evaluating the rate of false positive tags, which is denoted as "mistag" in this article. Mismeasurements are supposed to occur randomly; therefore the L_{xy} distribution of fake tags is expected to be symmetric with respect to the primary vertex.

B. Neural Network b-Tagging

As discussed in the previous section, SECVTX b-tagging depends on the long lifetime of B hadrons. D hadrons originating from c-quarks also have fairly long lifetime, and secondary vertices in c-jets are frequently tagged. Therefore jets tagged by SECVTX are still contaminated by falsely tagged gluon jets, light flavor (uds) jets, or c-jets[36]. A neural network has been developed to filter the b-tagging results(NNbtag) for the sake of improving the b-tagging purity [12].

The neural network used in this article employs the JETNET[13] package. The tagger is designed with two neural networks in series. One is trained to separate b-jets from l-jets, and the other, b from c. Jets which pass a cut on both of the neural network outputs are accepted by the tagger. These neural networks are trained and applied only to events which are already tagged by the SECVTX algorithm. At present, the NN b-tagging is tuned to increase the purity of the SECVTX b-tagged jets. It should be a future improvement to develop a method to increase not only purity but also tagging efficiency by applying the tagger to the jets without identified secondary vertices.

The neural networks take as input the 16 variables listed in Table I; distributions of the variables in simulated $t\bar{t}$ events are shown in Figs.4 and 5. Those variables are chosen primarily because the b-quark jets have higher track multiplicity, larger invariant mass, longer lifetime and harder fragmentation function than c- and l-quarks. The energy/momentum, track quantities and L_{xy} significance are good discriminators for b-jets. The p_T ratio variables are useful for identifying l-jets; however c-jets have p_T spectra similar to b-jets. Pseudo-$c\tau$ and vertex fit χ^2 are the best discriminators. The outputs of the two neural networks are shown in Fig 6.

The neural network b-tagger discussed above is validated by comparing the performance on data and Monte Carlo events. The neural network output from b-l network on a sample of SECVTX tagged heavy-flavor jets from the 8 GeV electron data and the corresponding Monte Carlo sample are shown in Fig.7, and the output from b-c network on a tagged light-flavor jets from generic jet data and Monte Carlo is also shown there. [37] Fig 7 shows the good agreement in neural network b-tagger performance between data and Monte Carlo.

The true b-jet selection efficiency for b, c and l jets as a function of the two neural network outputs are shown in Fig. ??. We choose to set the cut value for 90% b efficiency (after the SECVTX efficiency), corresponding to a value of $NN_{bl} = 0.182$ and $NN_{bc} = 0.242$. The scale factor, measured from the electron sample, is 0.97 ± 0.02 (Note that this is the additional scale factor on top of the SECVTX scale factor, and applicable because all of the jets under consideration have already been tagged by SECVTX). At these cut values, the neural network filter rejects 65% of light-flavor jets and about 50% of the c jets while keeping 90% of b-jets.

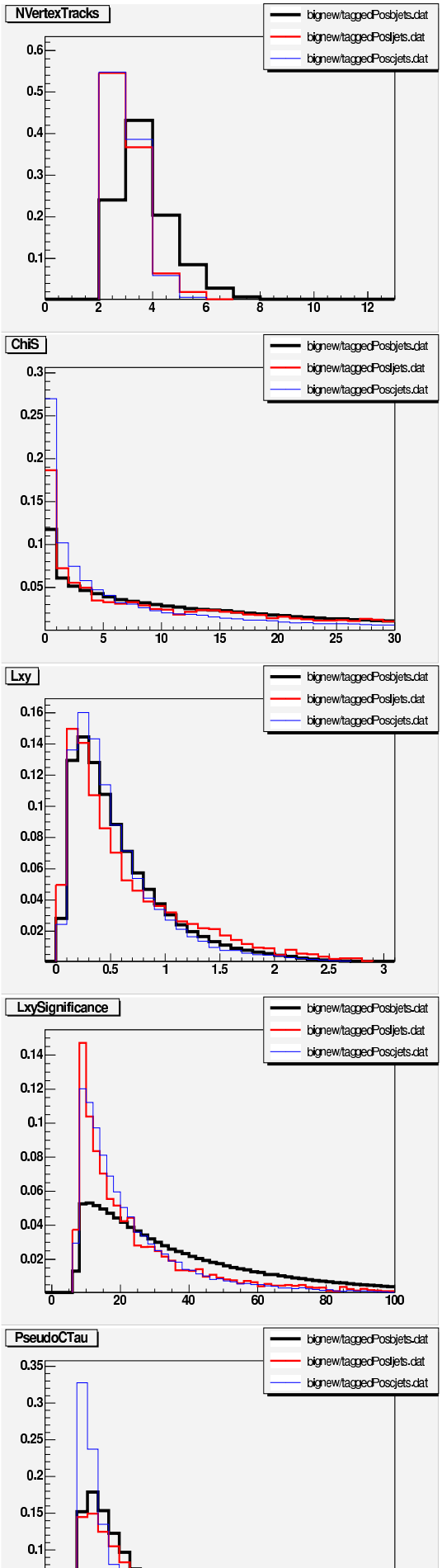

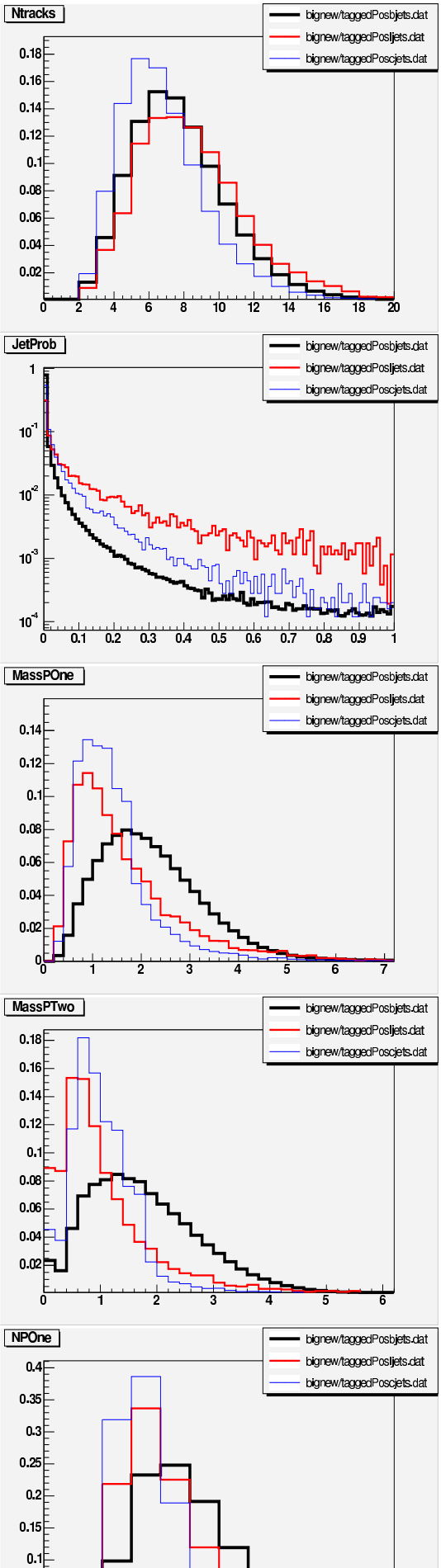

SECVTX variable	SECVTX independe
• Number of tracks in SECVTX	• Number of good track
• Fit χ^2	• Jet Probability (JetP
• Transverse decay length (L_{xy})	• Reconstructed mass o
• L_{xy} significance ($L_{xy}/\sigma_{L_{xy}}$)	• Reconstructed mass o
• Pseudo-$c\tau$ ($L_{xy} \times M_{SECVTX}/p_T^{SECVTX}$)	• Number of pass 1 trac
• Vertex Mass ($\sqrt{(\sum \lvert\boldsymbol{p}_{\rm vtx}\rvert)^2 - (\sum \boldsymbol{p}_{\rm vtx})^2}$)	• Number of pass 2 trac
• $p_T^{\rm vtx}/(\sum_{\rm good\ tracks} p_T)$	• $\sum_{\rm Pass1\ track} p_T/p_T^{jet}$
• Vertex pass number (pass 1 or 2)	• $\sum_{\rm Pass2\ track} p_T/p_T^{jet}$

TABLE I: Variables used in the neural network b-tagger.

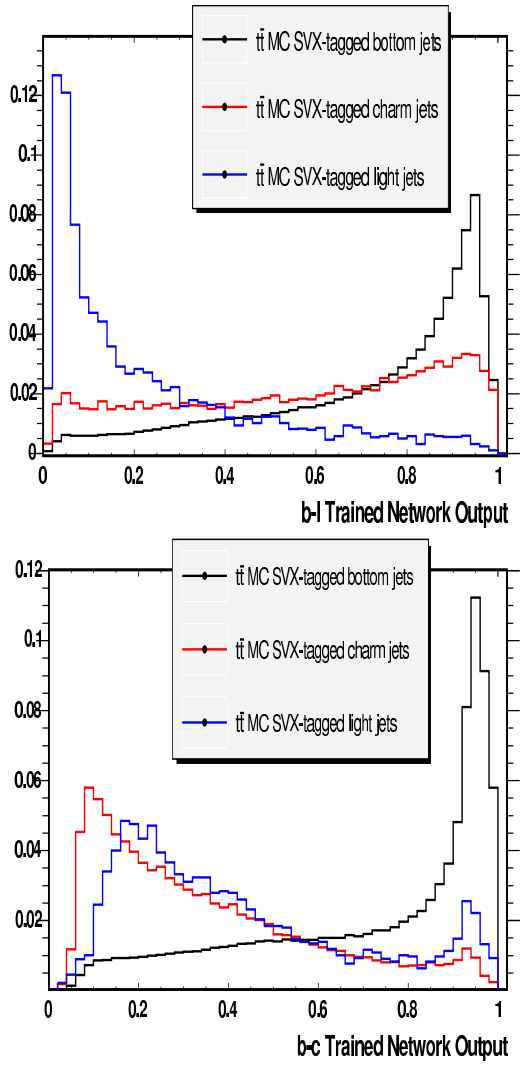

FIG. 6: Neural network outputs obtained from trainings of b-l(left) and b-c(right) jets. b, c and l jets are written in black, red and blue, respectively.

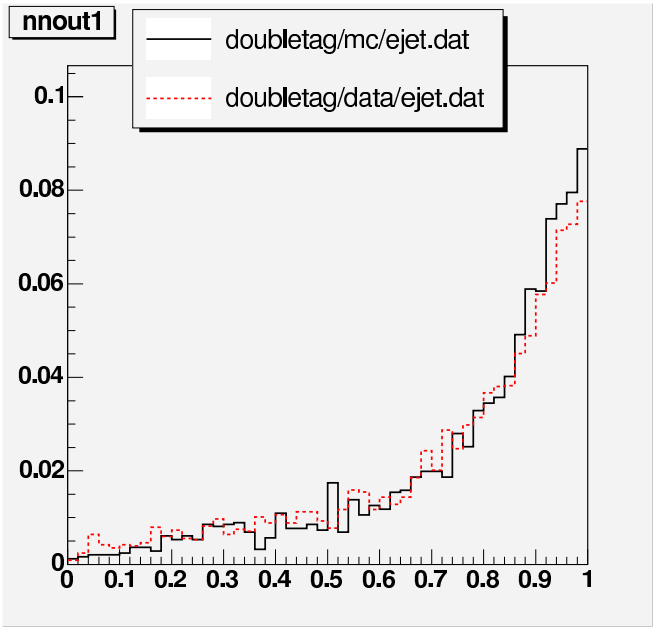

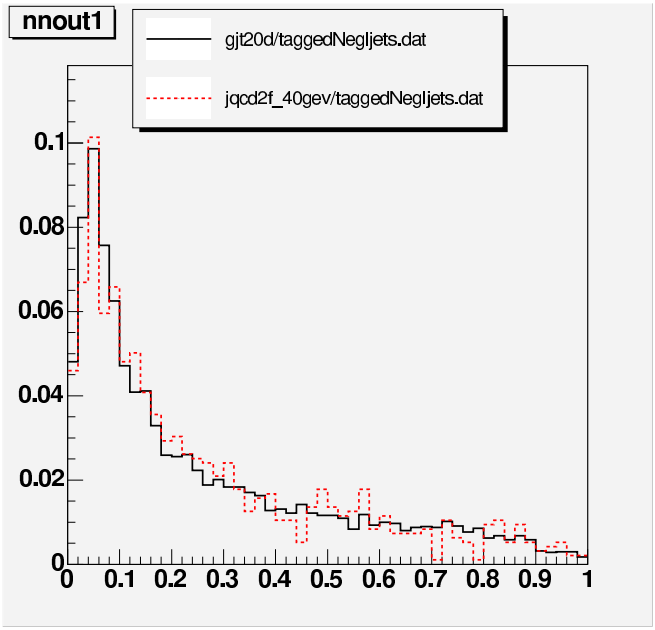

FIG. 7: Comparisons of NN b-tag output in data (solid black), and Monte Carlo (dashed red) for SECVTX-tagged heavy-flavor-enriched jets (left) and tagged light-flavor jets (right).

C. Muon

Muons are measured in subsystems outside the calorimeters, denoted CMU, CMP, CMX and IMU. Muon candidates are subdivided into several categories according to the detector subsystems that they propagate through. Muons that produce stubs in both CMU and CMP chambers are called CMUP muons. [38] The coverage of muon subsystems is different and the muons that have a stub in either CMU or CMP are labeled CMU-only or CMP-only muons. Muons that traverse and create a stub in CMX are called CMX muons.

D. Jet

Jet clustering starts with the most energetic calorimeter tower in a cluster, called a seed tower, and computes the energy sum in a cone of a given $\Delta R = \sqrt{\Delta\eta^2 + \Delta\phi^2}$. This analysis uses the cone size of $R = 0.4$. A jet "raw" four-momentum is then determined based on the energy of the cluster and the position of the energy-weighted centroid. Several corrections are applied to the raw quantities:

$$E_T^{\rm corr} = (E_T^{\rm raw} \times f_{\rm rel} \times -E_T^{\rm MI}) \times f_{\rm abs} - E_T^{\rm UE} + E_T^{\rm OC}, \quad (3)$$

where the corrections are the following:

- Level 1: relative correction, $f_{\rm rel}$, detector-η dependent, takes into account differences in tower-by-tower calorimeter response
- Level 2: time-dependent correction, $f_{\rm time}$, compensates for calorimeter deterioration over time, due, for instance, to aging of the photo-tubes
- Level 3: raw energy scale, $f_{\rm scale}$, accounts for non-linearities in single-particle
- Level 4: multiple interactions, $E_T^{\rm MI}$, correct for the possibility of several interactions in a particular bunch-crossing, parametrized by the number of vertices in the event
- Level 5: absolute energy correction, $f_{\rm abs}$, a p_T-dependent factor obtained from the Monte Carlo as a mean ratio of parton p_T to the jet p_T
- Level 6: underlying event, $E_T^{\rm UE}$, accounts for any contributions to the jet energy not coming from the original parton, beam remnants, spectator partons
- Level 7: out-of-cone correction, $E_T^{\rm OC}$, parametrized by p_T and determined from Monte Carlo, accounts for the energy deposited outside of the cone due to gluon radiation and fragmentation effects

E. Missing Transverse Energy

The "missing transverse energy" or $\not\!\!E_T$ is a reconstructed quantity that is not directly related to a single particle produced in a collision. Uncorrected $\not\!\!E_T$ is simply the opposite of the vector sum of all calorimeter tower depositions projected on the transverse plane. The missing energy is often thought of as a measure of the sum of the transverse momenta of the particles that escape detection, most notably neutrinos. To be more readily

interpretable as such, the raw $\not\!\!E_T$ needs to be corrected as follows:

$$\not\!\!\boldsymbol{E}_T^{\rm corr} = \not\!\!\boldsymbol{E}_T^{\rm raw} - \sum_{\rm jets} \left(\boldsymbol{E}_{T\rm jet}^{\rm corr} - \boldsymbol{E}_{T\rm jet}^{\rm raw} \right), \qquad (4)$$

where $\boldsymbol{E}_{T\rm jet}^{\rm corr}$, $\boldsymbol{E}_{T\rm jet}^{\rm raw}$ are transverse energy of jets before and after the jet energy correction, and $\not\!\!\boldsymbol{E}_T^{\rm raw}$ is a raw level missing E_T defined as:

$$\not\!\!\boldsymbol{E}_T^{\rm raw} = - \sum_{i \in \rm tower} \boldsymbol{E}_T^{(i)}, \qquad (5)$$

with $\boldsymbol{E}_T^{(i)}$ the transverse energies of any calorimeter towers.

IV. EVENT SELECTION

The experimental observable final state objects from $WH \to \ell\nu b\bar{b}$ are a lepton($e^{\pm}/\mu^{\pm}$), two jets, and missing E_T. WH events are expected to have high lepton p_T and large missing E_T because the W boson energy is split between the lepton and neutrino. To ensure a clean $WH \to \ell\nu b\bar{b}$ sample, high-p_T electron and muon triggers are used and additional offline selection criteria are imposed.

A. Triggers

In the electron trigger at Level 1, calorimeter towers are gathered in pairs so that the effective $\eta \times \phi$ segmentation is $0.2 \times 15^{\circ}$. At least one trigger tower is required to have $E_T > 8$ GeV with $E_{\rm HAD}/E_{\rm EM} < 0.125$. At least one XFT track with $p_T > 8$ GeV/c is also required to point to this tower. At Level 2, a clustering algorithm combines the energy deposited in neighboring towers. Towers adjacent to the seed tower found at Level 2 with $E_T > 7.5$ GeV are added to the cluster. The total E_T of the cluster must be larger than 16 GeV. At Level 3, full event reconstruction and electron identification are performed. A three dimensional COT track of $p_T > 9$ GeV must point to a cluster of $E_T > 18$GeV with $E_{\rm HAD}/E_{\rm EM} < 0.125$. This trigger is denoted by "ELECTRON_CENTRAL_18"

In the CMUP muon trigger at Level 1, hits in the CMU to match hits in the CMP are required. An XFT track with $p_T > 4$ GeV/c must point to the CMU and CMP hits. At Level 2, an XFT track with $p_T > 8$ GeV/c, which does not necessarily match the muon hits, has to exist. At Level 3, a fully reconstructed COT track with $p_T >$ 18 GeV/c must match a stub in the CMU($|\Delta x|_{\rm CMU} <$ 10 cm) and in the CMP($|\Delta x|_{CMP} < 20$ cm). This trigger is called "MUON_CMUP18".

In the CMX muon trigger at Level 1, CMX hits must match the central muon extension scintillator hits and an XFT track with $p_T >$8 GeV/c. At Level 2, no requirement is imposed. At Level 3, a fully reconstructed COT track with $p_T > 18$ GeV/c must match a stub in the CMX($|\Delta x|_{\rm CMX} < 10$ cm). This trigger is called "MUON_CMX18".

B. Offline Selections

Events are considered as WH candidates if they have exactly one primary lepton($e^{\pm}/\mu^{\pm}$). If there is more than one high-p_T leptons, the event is vetoed. The distance between the primary vertex and the lepton track z_0 must be less than 5 cm. This ensures the lepton and the tagge b jets come from the same hard interaction. To remove Z^0 events where one lepton daughter is unidentified, we reject events if the invariant mass of the lepton and any other object falls in the Z^0-boson mass window($76 < m_{\ell X} < 106$ GeV/c^2). The events are required to have large missing E_T, greater than 20 GeV. This requirement, along with the lepton requirement, satisfies the W selection.

The WH signal contains two jets originating from $H \to b\bar{b}$ decays. Thus the jets are expected to have large transverse energy, and they are required to be in the SVX coverage for SECVTX b-tagging. Specifically, we require jets to satisfy $E_T > 15$ GeV and $|eta| < 2.0$. For the search for $WH \to \ell\nu b\bar{b}$, $W+$ exactly 2 jets events are used. However, W+1,3,$\geq$4 jet events also gives a good cross checks of the data handling and background modeling considered in the next chapter.

To increase the signal purity of the W+2-jet events, at least one jet must be b-tagged by the SECVTX algorithm. If only one of the jets is b-tagged, the jet is also required to pass the neural network b-tagging filter to reject mistag, $Wc\bar{c}$ and Wc events. If there are two or more SECVTX b-tagged jets, neural network is not applied. Such events are already rather pure, because it is rare that two or more jets are mistagged by SECVTX simultaneously.

C. Luminosity

The results presented here use data collected between February 2002 and February 2006. Due to some inefficiency in specific portions of detectors, the total luminosities differ from detector to detector as listed in Table II. In this article, the total luminosity is denoted by 955 pb^{-1} or 1fb^{-1}, depending on the context.

V. BACKGROUND

The final state signature from $WH \to \ell\nu b\bar{b}$ production – lepton ($e^{\pm}/\mu^{\pm}$)+ two jets + large missing E_T – can also be reached from other production processes.

Detector	Integrated luminosity(pb^{-1})
CEM	955 ± 57
CMUP	955 ± 57
CMX (arch)	941 ± 56
CMX (keystone, miniskirt)	622 ± 37

TABLE II: Integrated luminosity breakdown by subdetector.

These background processes include $t\bar{t}$ production, non-resonant W+jets production, and non-W QCD production. Several electroweak production processes also contribute small background rates. The exact composition of the W+jets sample depends on the number of jets required.

In the following subsections, the contribution from each background source is calculated in detail.

A. Non-W QCD

Events from generic QCD production sometimes mimic the W-boson signature with fake leptons or fake missing E_T. Non-W leptons are reconstructed when a jet passes the lepton selection criteria based on calorimeter based measurement or a heavy flavor jet produces leptons via semileptonic decay. Non-W missing E_T can be observed via mismeasurements of energy or semileptonic decays of heavy flavor jet can be obtained. It is difficult to model and produce such events in detector simulation since the reasons for mismeasurement are not entirely known.

Generally, non-W events come from a non-isolated lepton[39] and small missing E_T. This event model is used to extrapolate the expected non-W contribution into the signal region, e.g. good lepton isolation and large missing E_T. Specfically, let isolation vs missing E_T plane be divided into the following 4 sectors (shown in Fig.8)[14, 15]:

- region A: Isolation > 0.2 and $\not\!\!E_T < 15$ GeV
- region B: Isolation < 0.1 and $\not\!\!E_T < 15$ GeV
- region C: Isolation > 0.2 and $\not\!\!E_T > 20$ GeV
- region D: Isolation < 0.1 and $\not\!\!E_T > 20$ GeV

Here, region D corresponds to the signal region. The distribution of missing E_T vs isolation in high-p_T electron and muon samples are shown in Fig.9. In extracting the non-W background contribution from data, we make a the following assumptions: lepton isolation and missing E_T are uncorrelated in non-W events, and the b-tagging rate is not dependent on missing E_T in non-W events. Since lepton and missing E_T in non-W events are not real, there is no reason for them to be correlations. Also b-tagging, which depends only on vertex-finding among charged tracks, should not be affected too much by missing E_T.

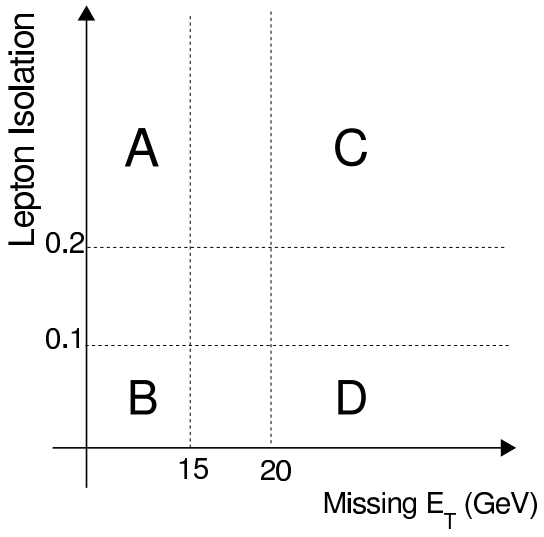

FIG. 8: Missing E_T and lepton isolation plane divided into four sectors for non-W background estimation.

With the first assumption, the number of non-W events($N_D^{\text{non}-W}$) and the fraction($f_{\text{non}-W}$) in the signal region before requiring b-tagging follow the relation

$$N_D^{\text{non}-W} = \frac{N_B \times N_C}{N_A}, \quad (6)$$

$$f_{\text{non}-W} = \frac{N_D^{\text{non}-W}}{N_D} = \frac{N_A \times N_B}{N_C \times N_D}, \quad (7)$$

where N_i $(i = A, B, C, D)$ are the number of pretag events in each sideband region. In accordance with the second assumption, the SECVTX b-tagging efficiency obtained in region B can be applied to the signal region D. Here we define an event tagging efficiency per taggable jets as:

$$r_B = \frac{N_B^{(\text{tagged event})}}{N_B^{(\text{taggable jet})}}, \quad (8)$$

where $N_B^{(\text{tagged event})}$ and $N_B^{(\text{taggable jet})}$ are number of tagged events and taggable jets in region B respectively. Then the number of non-W background in region D after SECVTX b-tagging($N_D^{+\text{non}-W}$) is obtained by using the "Tag Rate" relation:

$$N_D^{+\text{non}-W} = f_{\text{non}-W} \times r_B \times N_D^{(\text{taggable jets})}. \quad (9)$$

It is also possible to estimate non-W contribution solely

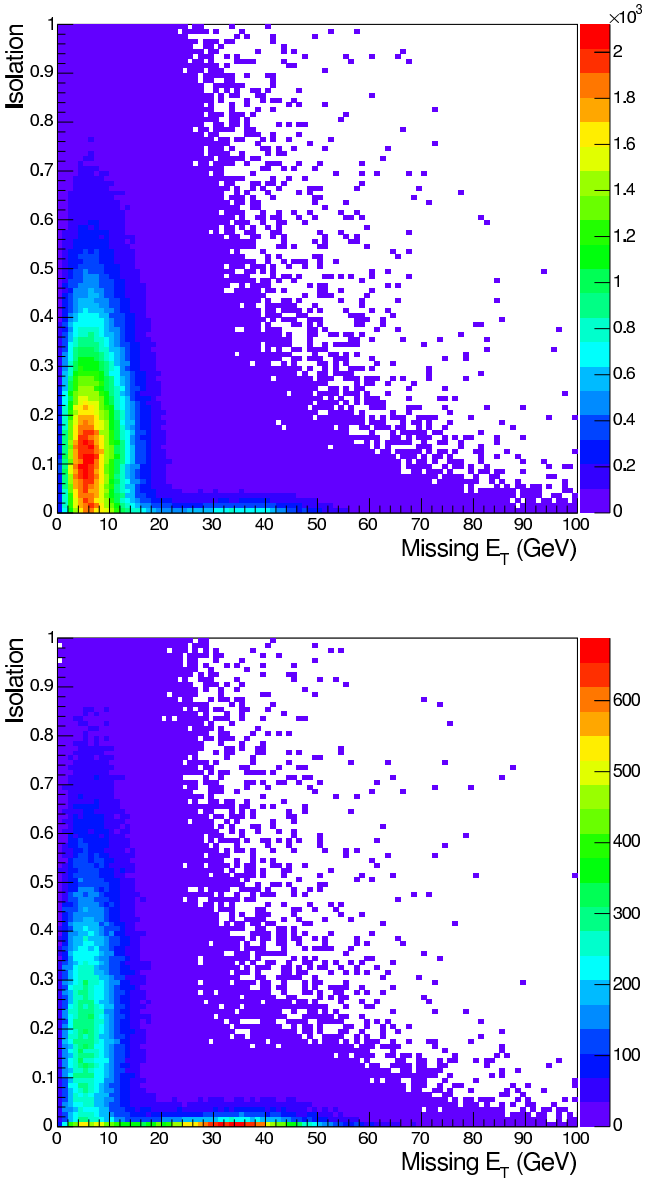

FIG. 9: Missing E_T vs lepton isolation distributions in high-p_T electron(left) and muon(right) samples associated with at least one jet before applying SECVTX b-tagging.

from the SECVTX-tagged sample as:

$$N_D'^{+\text{non}-W} = \frac{N_B^+ \times N_C^+}{N_A+}, \tag{10}$$

where $N_X^+(X = A, B, C, D)$ in the "Tagged Method" are the number of positively SECVTX b-tagged events. These methods are data-based techniques, so the estimates could also contain other background processes. The contributions from $t\bar{t}$ and W+jets events to each sideband region are studied in [14, 15], and their contributions from $t\bar{t}$ and W+jets events to each side band region are subtracted.

To validate the four-sector method and estimate the systematic uncertainties , the following control sectors are considered:

- region A: Isolation > 0.2 and $\not\!\!E_T < 15$ GeV
- region E: $0.1 <$ Isolation < 0.2 and $\not\!\!E_T < 15$ GeV
- region C: Isolation > 0.2 and $\not\!\!E_T > 20$ GeV
- region F: $0.1 <$ Isolation < 0.2 and $\not\!\!E_T > 20$ GeV
- region A'': Isolation > 0.1 and $\not\!\!E_T < 10$ GeV
- region A' : Isolation > 0.1 and $10 < \not\!\!E_T < 20$ GeV
- region B'': Isolation < 0.1 and $\not\!\!E_T < 10$ GeV
- region B' : Isolation < 0.1 and $10 < \not\!\!E_T < 20$ GeV

These regions are slightly different from what was considered in the non-W estimation. They can be used to see the effects, *e.g. stability and systematic uncertainty*, when the boundaries of the four sectors are varied. The ratios $G = (N_E \cdot N_C)/(N_A \cdot N_F)$ and $G' = (N_{B''} \cdot N_{A'})/(N_{A''} \cdot N_{B'})$ are calculated for both pretag and tagged samples. Here region F and B' are the isolation and missing E_T sideband region. If the extrapolations from isolation and missing E_T are valid, the fractions of G and G' should be equal to unity. Deviations from unity are assigned as systematic uncertainty, so a 25% systematic uncertainty is assigned conservatively for both the pretag and tagged estimate.

The independent estimate from the tag rate method and the tagged method are combined in a weighted average. At first the estimates over the different lepton categories for each method are added, then these two methods are combined. The final non-W estimates are shown in **Table III** for events with at least one SECVTX b-tagged jet. The result from tagged method gives a slightly higher estimate than tag rate method, but those results are consistent within uncertainties.

When neural network b-tagging filter is applied, a non-W rejection factor is measured from data in region C. Region C has event kinematics similar to real non-W events in the signal region D because lepton isolation is the only difference between the two regions. The non-W estimate calculated before applying NN b-tagging is scaled by this NN rejection factor.

The non-W estimate for events with at least two SECVTX tags is obtained by measuring the ratio of the number of events with at least one b-tag to that with at least two b-tag in region A'(Isolation > 0.1 and $10 < \not\!\!E_T < 20$ GeV), B, and C'(Isolation > 0.1 and $\not\!\!E_T > 20$ GeV) because just a few events remain after requiring at least two SECVTX b-tagging. The non-W estimate for at least two SECVTX b-tagging is obtained by applying the ratio to the estimate with at least one SECVTX b-tagging. The non-W background estimates for various b-tagging strategies are summarized in Table IV.

Jet Multiplicity	1jet	2jet	3jet	≥4jet
TagRate	124.6 ± 25.8	56.9 ± 12.1	16.3 ± 3.6	6.5 ± 1.5
Tagged	206.1 ± 54.7	76.5 ± 22.4	24.1 ± 9.4	20.8 ± 12.0
Combined	139.1 ± 23.3	61.3 ± 10.7	17.3 ± 3.4	6.7 ± 1.5

TABLE III: Summary of non-W background estimate as a function of jet multiplicity for events with at least one SECVTX b-tagged jet.

Jet Multiplicity	1jet	2jet	3jet	≥4jet
≥1 SECVTX	139.1 ± 23.3	61.3 ± 10.7	17.3 ± 3.4	6.7 ± 1.5
= 1 SECVTX	139.1 ± 23.3	59.9 ± 10.4	16.4 ± 3.2	6.4 ± 1.4
= 1 SECVTX & NN tag	84.2 ± 14.1	38.9 ± 6.7	12.1 ± 2.3	5.5 ± 1.2
≥ 2 SECVTX	-	1.4 ± 0.3	0.9 ± 0.2	0.3 ± 0.1

TABLE IV: Summary of non-W background estimate as a function of jet multiplicity for various b-tagging options.

B. Mistagged Jets

The rate at which SECVTX falsely-tags light flavor jets is derived from generic jet samples in varying bins of η, ϕ, jet E_T, track multiplicity[16]. Tag rate probabilities are summed for all of the taggable jets in the event. Since the double mistag rate is small, this sum is a good approximation of the single-tag event rate. Negative mistags – tags with unphysical negative decay length due to finite tracking resolution – are calculated as a good estimate of falsely tagged jets, independent to first order of heavy flavor content in the generic jet sample. An 8% systematic uncertainty on the rate is largely due to self-consistency in the parameterization as applied to the generic jet sample. The positive mistag rate is enhanced relative to the negative tag rate by light-flavor secondary vertices and material interactions in the silicon detectors. The positive mistag rate is corrected by multiplying the negative mistag rate by a factor of 1.37 ± 0.15 [17]. For data collected after December 2004, an additional correction factor of 1.05 ± 0.03 [18] is applied. The mistag rate per jet is applied to events in the W+jets sample. The total estimate is corrected for the non-W QCD fraction and also the $t\bar{t}$ contribution to the pretag sample. To estimate the mistag contribution in NN-tagged events, we apply the light flavor rejection power of the b-tagger 0.35 ± 0.05. The mistag estimate for various b-tagging strategies are summarized in Table V.

C. W+Heavy Flavor

The $Wb\bar{b}$ and $Wc\bar{c}$ states are major background sources of b-tags in the W+jets channel. Rates for these processes are normalized to data because current Monte Carlo programs can generate W+heavy flavor events only to leading order. As a result, large theoretical uncertainties exist for the overall normalization. The contribution from true heavy flavor production in W+jet events is determined from measurements of the heavy flavor event fraction in W+jet events and the b-tagging efficiency for those events.

The fraction of W+jets events produced with heavy flavor jets has been studied extensively [19] using an ALPGEN + HERWIG combination of Monte Carlo programs [20, 21]. Calculations of the heavy flavor fract in ALPGEN have been calibrated using a jet data sample, and measurements indicate a scaling factor of 1.5 ± 0.4 is necessary to make the heavy flavor production in Monte Carlo match the production in data. The final results of heavy flavor fractions are obtained as shown in **Table VI.** In the table, 1B and 1C refer to the case in which only one of the heavy flavor jets are detected; this happens when one jet goes out of the detector coverage or when two parton jets merge into the same reconstructed jet. Similarly, 2B and 2C refer to the case in which both of the heavy flavor jets are observed.

For the tagged W+HF background estimate, the heavy flavor fractions and tagging rates given in Tables VI and VII are multiplied by the number of pretag events in data, after correction for the contribution of non-W and $t\bar{t}$ events to the pretag sample.

A previous analysis using 319 pb^{-1} of data provided evidence that the disagreement between the predicted and observed numbers of W+1jet and W+2jet events is due to the heavy flavor fraction [5]. In this analysis, the same correction factor of 1.2 ± 0.2, obtained by fitting W+1jet events, is applied to the heavy flavor fraction. Finally, the W+HF background contribution is obtained by the following relation:

$$N_{W+HF} = f_{HF} \cdot \epsilon_{\rm tag} \cdot [N_{\rm pretag} \cdot (1 - f_{\rm non-}{}_W) - N_{\rm EWK}], \quad (11)$$

where f_{HF} is heavy fraction, $\epsilon_{\rm tag}$ is tagging efficiency and $N_{\rm EWK}$ is the expected number of $t\bar{t}$, single top and dibo-

Jet Multiplicity	1jet	2jet	3jet	≥4jet
≥ 1 SECVTX tag	399.0 ± 63.0	163.5 ± 25.8	49.2 ± 7.8	15.2 ± 2.4
= 1 SECVTX tag	399.0 ± 63.0	159.9 ± 25.3	47.2 ± 7.5	14.0 ± 2.2
= 1 SECVTX & NN tag	139.7 ± 27.3	53.9 ± 10.7	15.7 ± 3.1	4.2 ± 0.8
≥ 2 SECVTX tag	-	3.5 ± 0.5	2.0 ± 0.3	1.2 ± 0.2

TABLE V: Summary of mistag background estimate for various b-tagging strategies.

son events. The W+heavy flavor background estimate is summarized in Table VIII.

D. Electroweak Backgrounds

The normalization of the diboson and single top backgrounds are based on the theoretical cross sections listed in Table IX, the measured luminosity and the acceptance and b-tagging efficiency derived from MC [22–25]. The MC acceptance is corrected for lepton identification, trigger efficiencies and z vertex cut. The tagging efficiency is always corrected by the scale factor (MC/data) of 0.89± 0.07. The expected number of events is obtained by the equation

$$N = \int \mathcal{L}dt \times \epsilon \times \sigma, \tag{12}$$

where ϵ is the total detection efficiency corrected by all of the scale factors.

E. Summary of Background Estimate

We have described the contributions of individual background sources to the final background estimate. The summary of the background estimates for the b-tagging condition of exactly one b-tagged jet before and after applying NN filter and at least two SECVTX b-tagged jets are shown in Tables X, XI, Figs.10 and 11. The observed number of events in the data and the Standard Model background expectations are consistent before and after neural network b-tagging is applied. The same is true for the number of events with at least two b-tagged jets. (See Table XII and Fig. 11.)

VI. HIGGS BOSON SIGNAL ACCEPTANCE

The kinematics of the $WH \to \ell\nu b\bar{b}$ process are well-defined by the Standard Model and events can be generated by Monte Carlo programs. In this article, PYTHIA is used to generate the signal samples [26]. However, the Standard Model Higgs boson mass is an unknown input parameter. The Higgs boson branching ratio is dominated by the mode $H \to b\bar{b}$ for $m_H > 135$ GeV/c^{2}and by $H \to W^+W^-$ for $m_H > 135$ GeV/c^2. In this analysis, only Higgs boson masses between 110 and 150 GeV/c^2 are considered. The number of expected $WH \to \ell\nu b\bar{b}$ events($N_{WH\to\ell\nu b\bar{b}}$) is obtained by:

$$N_{WH\to\ell\nu b\bar{b}}(m_H) = \epsilon_{WH\to\ell\nu b\bar{b}}(m_H) \cdot \int dt\mathcal{L} \cdot \sigma(p\bar{p} \to WH|m_H) \cdot Br(H \to b\bar{b}), \tag{13}$$

where $\epsilon_{WH\to\ell\nu b\bar{b}}$, $\int dt\mathcal{L}$, $\sigma(p\bar{p} \to WH)$ and $Br(H \to b\bar{b})$ are the event detection efficiency, integrated luminosity, production cross section and branching ratio, respectively. The production cross section and branching ratio are calculated to the NLO precision at considered Higgs boson mass points [3, 4]. The acceptance $\epsilon_{WH\to\ell\nu b\bar{b}}$ is broken down into the following factors:

$$\epsilon_{WH\to\ell\nu b\bar{b}} = \epsilon_{z_0} \cdot \epsilon_{\text{trigger}} \cdot \epsilon_{\text{lepton ID}} \cdot \epsilon_{b\text{tag}} \cdot \epsilon_{\text{kinematics}} \cdot \left(\sum_{l'=e,\mu,\tau} Br(W \to l' \right. \tag{14}$$

where ϵ_{z_0}, $\epsilon_{\text{trigger}}$, $\epsilon_{\text{lepton ID}}$, $\epsilon_{b\text{tag}}$ and $\epsilon_{\text{kinematics}}$ are efficiencies to meet the requirements of primary vertex, trigger, lepton ID, b-tagging and kinematics. The factor ϵ_{z_0} is obtained from data, and the others are calculated using Monte Carlo samples. The overall acceptances for various b-tagging options including all systematic uncertainties as a function of Higgs boson mass are shown in Fig.12.

The expected number of $WH \to \ell\nu b\bar{b}$ signal events is estimated by Eq.13 at each Higgs boson mass point. The expectations for various b-tagging strategies are shown in Table XIII. Neural Network b-tagging keeps about 90% of signal acceptance while it reduces about 65% of total background in W+2jet events according to Tables X and XI.

The systematic uncertainties on the acceptance stems from the jet energy scale, initial and final state radiation, lepton identification, trigger efficiencies and b-tagging scale factor. Individual sources of systematic uncertainty are discussed in detail.

A 2% uncertainty on the lepton identification efficiency is assigned for each lepton type (CEM electron, CMUP and CMX muon), based on studies of Z boson events [27–30]. For each of the high p_T lepton triggers, a 1% uncertainty is measured from backup trigger paths or Z boson events [31, 32]. The initial and final state radition systematic uncertainties are estimated by changing the parameters related to ISR and FSR from nominal values to half and double. The difference from the nominal acceptance is taken as the systematic uncertainly. The

Jet Multiplicity	1jet	2jet	3jet	≥ 4 jet
W+HF fraction before tagging (%)				
$WBB(1B)$	1.0 ± 0.3	1.4 ± 0.4	2.0 ± 0.5	2.2 ± 0.6
$WBB(2B)$	0.0 ± 0.0	1.4 ± 0.4	2.0 ± 0.5	2.6 ± 0.7
$WCC(1C)$	1.6 ± 0.4	2.4 ± 0.6	3.4 ± 0.9	3.6 ± 1.0
$WCC(2C)$	0.0 ± 0.0	1.8 ± 0.5	2.7 ± 0.7	3.7 ± 1.0
Wc	4.3 ± 0.9	6.0 ± 1.3	6.3 ± 1.3	6.1 ± 1.3

TABLE VI: The heavy flavor fractions in W + jets sample. Raw results from ALPGEN Monte Carlo have been scaled by the data-derived calibration factor of 1.5 ± 0.4. (Wc fractions have not been rescaled.)

Jet Multiplicity	1jet	2jet	3jet	$\geq$ 4jet
≥ 1 SECVTX b-tag				
$WBB(1B)$	33.2 ± 2.4	34.5 ± 2.5	36.7 ± 2.6	40.2 ± 2.9
$WBB(2B)$	-	51.3 ± 3.6	54.1 ± 3.8	55.1 ± 3.9
$WCC(1C)$	6.2 ± 0.9	8.0 ± 1.1	9.7 ± 1.4	11.6 ± 1.6
$WCC(2C)$	-	14.4 ± 2.0	17.0 ± 2.4	17.8 ± 2.5
WC	8.9 ± 1.3	8.7 ± 1.2	7.6 ± 1.1	3.4 ± 0.5
≥ 1 SECVTX and NN b-tag				
$WBB(1B)$	29.9 ± 2.1	31.8 ± 2.3	34.1 ± 2.4	35.9 ± 2.6
$WBB(2B)$	-	47.2 ± 3.4	51.5 ± 3.7	51.3 ± 3.6
$WCC(1C)$	3.8 ± 0.5	5.5 ± 0.8	6.1 ± 0.9	6.4 ± 0.9
$WCC(2C)$	-	9.9 ± 1.4	8.6 ± 1.2	9.5 ± 1.4
WC	5.0 ± 0.7	4.6 ± 0.7	3.1 ± 0.4	3.4 ± 0.5
≥ 2 SECVTX b-tag				
$WBB(2B)$	-	9.7 ± 0.7	13.6 ± 1.0	11.5 ± 0.8
$WCC(2C)$	-	1.2 ± 0.2	0.8 ± 0.1	0.9 ± 0.1

TABLE VII: The b-tagging efficiencies by various b-tagging strategies for individual W+heavy flavor processes. Those numbers include the effect of the scale factors of SECVTX and NN b-tagger.

uncertainty in the incoming partons' energies relies on the eigenvectors provided in the PDF fits. An NLO version of the PDFs, CTEQ6M, provides a 90% confidence interval of each eigenvector. The nominal PDF value is reweighted to the 90% confidence level value, and the corresponding acceptance is computed. The differences between nominal and reweighted acceptances are added in quadrature, and the total is assigned as the systematic uncertainty.

The uncertainty due to the jet energy scale uncertainty [**?**] is calculated by shifting jet energies in WH Monte Carlo samples by $\pm 1\sigma$. The deviation from the nominal acceptance is taken as the systematic uncertainty. The systematic uncertainty on the SECVTX b-tagging efficiency is based on the scale factor uncertainty discussed in Sec.III A. When Neural Network b-tagging is applied, the scale factor uncertainty from NN b-tagging(see Sec.III B) is added to that of SECVTX in quadrature.

The total systematic uncertainties for various b-tagging options are summarized in Table XIV.

VII. INTERPRETATION OF RESULTS

The search strategy is optimized by calculating a significance defined as $S/\sqrt{B}$ where S and B are the number of expected signal and background events. In this analysis, S and B are counted within a window which gives the best significance in dijet mass distribution. The window itself is optimized by varying the window peak and width for each b-tagging strategy. A comparison of significance between various b-tagging options, shown in Fig.13, provides an *a priori* metric that predicts which selection gives the best result.

The improvement from the Neural Network b-tagging is seen in the significances. Requiring the NN filter improves the sensitivity by about 10% in the sample of events with exactly one b tag. The significance in double-tagged events is almost the same as that in events with at

Jet multiplicity	1jet	2jet	3jet	$\geq$ 4jet
		≥ 1 SECVTX b-tag		
$Wb\bar{b}$	340.9 ± 118.3	179.0 ± 61.2	37.8 ± 12.3	8.0 ± 3.2
$Wc\bar{c}$	101.6 ± 35.3	67.1 ± 22.9	16.4 ± 5.3	3.7 ± 1.5
Wc	325.7 ± 82.8	65.1 ± 17.0	8.3 ± 2.2	0.6 ± 0.2
		$= 1$ SECVTX b-tag		
$Wb\bar{b}$	340.9 ± 118.3	158.7 ± 54.2	32.1 ± 10.5	7.0 ± 2.8
$Wc\bar{c}$	101.6 ± 35.3	63.8 ± 21.8	16.0 ± 5.2	3.6 ± 1.5
Wc	325.7 ± 82.8	65.1 ± 17.0	8.3 ± 2.2	0.6 ± 0.2
		$= 1$ SECVTX and NN b-tag		
$Wb\bar{b}$	306.9 ± 106.9	144.7 ± 49.4	29.9 ± 9.7	6.4 ± 2.5
$Wc\bar{c}$	63.1 ± 22.0	43.0 ± 14.7	8.7 ± 2.8	1.9 ± 0.8
Wc	185.7 ± 47.2	34.4 ± 9.0	3.4 ± 0.9	0.6 ± 0.2
		≥ 2 SECVTX b-tag		
$Wb\bar{b}$	-	20.3 ± 7.0	5.7 ± 1.8	1.0 ± 0.4
$Wc\bar{c}$	-	3.3 ± 1.1	0.4 ± 0.1	0.1 ± 0.04
Wc	-	-	-	-

TABLE VIII: Summary of W+heavy flavor background estimate for various b-tagging options.

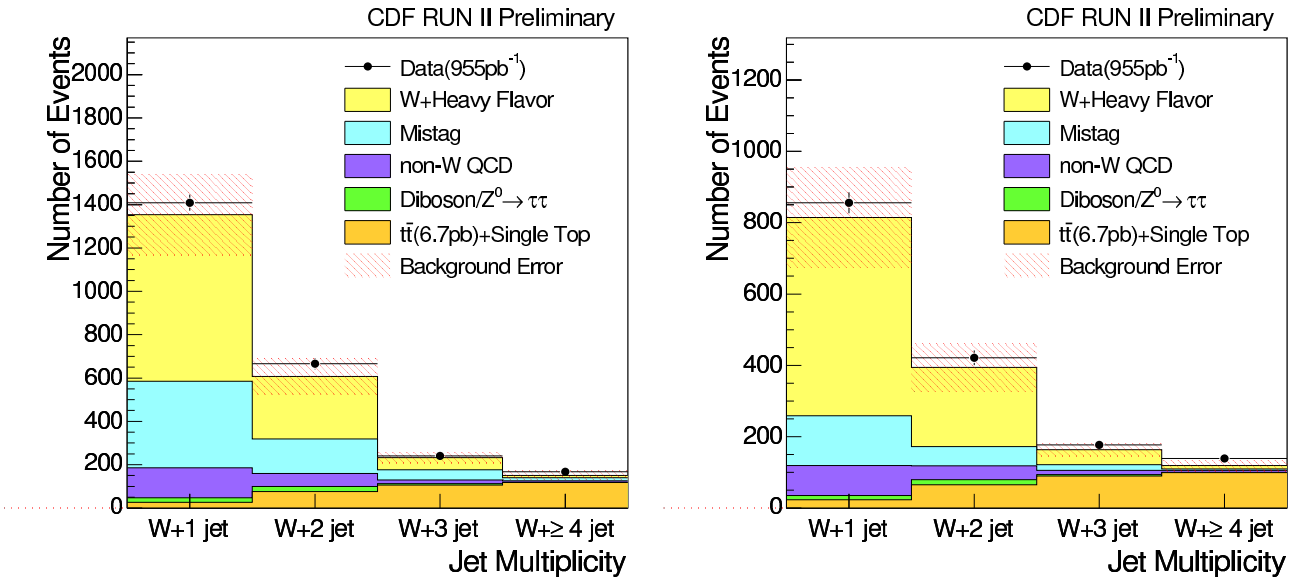

FIG. 10: Number of events as a function of jet multiplicity for events with exactly one SECVTX b-tag before(left) and after(right) applying the NN b-tagging requirement.

least one tag and no NN filter. Combining the two results yields another sensitivity improvement. The significance from the combination is calculated as:

$$\mathrm{Sig}(=1\mathrm{tag}\&\&\geq 2\mathrm{tag}) = \sqrt{\mathrm{Sig}(=1\mathrm{tag})^2 + \mathrm{Sig}(\geq 2\mathrm{tag})^2}. \quad (15)$$

This combined use of two separate b-tagged samples provides a significant improvement on the significance as shown in Fig.13. The improvement from "$\geq$ 1 tag && w/ NNtag" is about 20% compared to "= 1Tag w/ NN Tag && $\geq$ 2 Tag", which shows the best sensitivity without considering the combined use of two tagging conditions. Therefore, the final results come from events having exactly one SECVTX b-tagged jet with Neural Network filter or at least two SECVTX b-tagged jets.

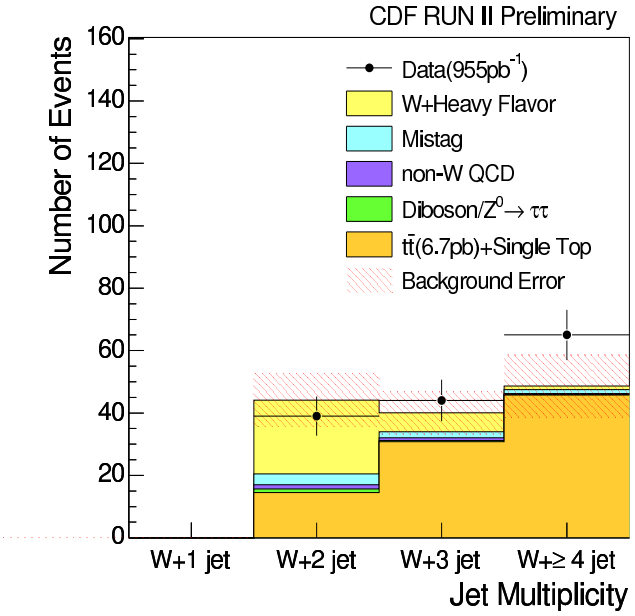

FIG. 11: Number of events as a function of jet multiplicity for events with at least two SECVTX b-tagged jets.

Theoretical Cross Sections	
WW	12.40 ± 0.8 pb
WZ	3.96 ± 0.06 pb
ZZ	1.58 ± 0.02 pb
Single Top s-channel	0.88 ± 0.05 pb
Single Top t-channel	1.98 ± 0.08 pb
$Z \to \tau\tau$	320 ± 9.0 pb
$t\bar{t}$	$6.7\ ^{+0.7}_{-0.9}$ pb

TABLE IX: Theoretical cross sections and errors for the electroweak and single top backgrounds, along with the theoretical cross section for $t\bar{t}$ at ($m_t = 175\text{GeV/c}^2$). The cross section of $Z^0 \to \tau\tau$ is obtained in the dilepton mass of $m > 30$ GeV/c^2 together with k-factor(NLO/LO) of 1.4.

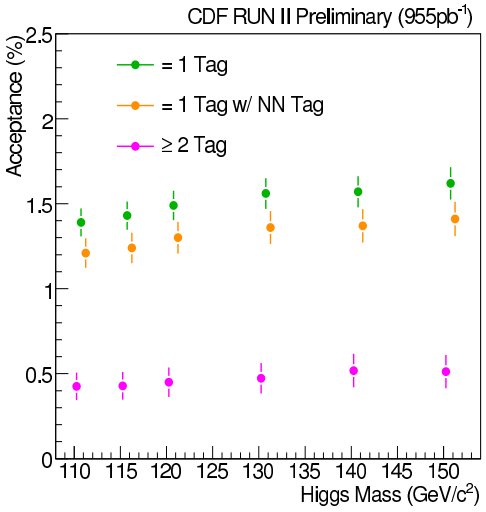

FIG. 12: The summary of acceptance of the process $WH \to \ell\nu b\bar{b}$ in W+2jet bin for various b-tagging strategies as a function of Higgs boson mass.

VIII. LIMIT ON HIGGS BOSON PRODUCTION

As shown in the previous section, there is no significant excess over the Standard Model background expectation. We set an upper limit on the WH production cross section times branching ratio. Dijet mass distributions are fit to extract an upper limit with a binned likelihood technique because the dijet mass resonance is a strong discriminant for the Higgs boson signature. After setting an upper limit from $WH \to \ell\nu b\bar{b}$, the limit is combined with other limits already obtained in CDF RUN II experiment. Finally, the combination between this CDF result and similar results from the DØ is also performed.

A. Binned Likelihood Technique

The data counts in each bin follow Poisson statistics. Let the Poisson probability be written as:

$$P_i(n_i, \mu_i) = \frac{\mu_i^{n_i} e^{-\mu_i}}{n_i!} \quad (i = 1, 2, \cdots, N_{\text{bin}}), \qquad (16)$$

Jet Multiplicity	1jet	2jet	3jet	$\geq$ 4jet
Pretag Events	94051	14604	2362	646
Mistag	399.0 $\pm$ 63.0	159.9 $\pm$ 25.3	47.2 $\pm$ 7.5	14.0 $\pm$ 2.2
$Wb\bar{b}$	340.9 $\pm$ 118.3	158.7 $\pm$ 54.2	32.1 $\pm$ 10.5	7.0 $\pm$ 2.8
$Wc\bar{c}$	101.6 $\pm$ 35.3	63.8 $\pm$ 21.8	16.0 $\pm$ 5.2	3.6 $\pm$ 1.5
Wc	325.7 $\pm$ 82.8	65.1 $\pm$ 17.0	8.3 $\pm$ 2.2	0.6 $\pm$ 0.2
$t\bar{t}$(6.7pb)	7.9 $\pm$ 1.4	49.2 $\pm$ 8.3	100.2 $\pm$ 16.9	116.8 $\pm$ 19.7
Single Top	19.1 $\pm$ 2.0	27.1 $\pm$ 2.9	5.6 $\pm$ 0.6	0.9 $\pm$ 0.1
Diboson/$Z^0 \rightarrow \tau\tau$	20.0 $\pm$ 3.3	23.3 $\pm$ 3.4	6.8 $\pm$ 1.4	1.7 $\pm$ 0.6
non-W QCD	139.1 $\pm$ 23.3	59.9 $\pm$ 10.4	16.4 $\pm$ 3.2	6.4 $\pm$ 1.4
Total Background	1353.3 $\pm$ 187.4	607.0 $\pm$ 83.6	232.6 $\pm$ 25.2	151.0 $\pm$ 20.5
Observed Events	1409	666	241	167

TABLE X: Background estimate for events with exactly one SECVTX b-tag as a function of jet multiplicity.

Jet Multiplicity	1jet	2jet	3jet	$\geq$ 4jet
Pretag Events	94051	14604	2362	646
Mistag	139.7 $\pm$ 27.3	53.9 $\pm$ 10.7	15.7 $\pm$ 3.1	4.2 $\pm$ 0.8
$Wb\bar{b}$	306.9 $\pm$ 106.9	144.7 $\pm$ 49.4	29.9 $\pm$ 9.7	6.4 $\pm$ 2.5
$Wc\bar{c}$	63.1 $\pm$ 22.0	43.0 $\pm$ 14.7	8.7 $\pm$ 2.8	1.9 $\pm$ 0.8
Wc	185.7 $\pm$ 47.2	34.4 $\pm$ 9.0	3.4 $\pm$ 0.9	0.6 $\pm$ 0.2
$t\bar{t}$(6.7pb)	6.9 $\pm$ 1.2	42.0 $\pm$ 6.6	84.9 $\pm$ 12.8	98.6 $\pm$ 14.3
Single Top	16.7 $\pm$ 1.8	23.5 $\pm$ 2.4	4.8 $\pm$ 0.5	0.8 $\pm$ 0.1
Diboson/$Z^0 \rightarrow \tau\tau$	11.7 $\pm$ 2.2	14.2 $\pm$ 2.3	3.9 $\pm$ 0.9	1.0 $\pm$ 0.3
non-W QCD	84.2 $\pm$ 14.1	38.9 $\pm$ 6.7	12.1 $\pm$ 2.3	5.5 $\pm$ 1.2
Total Background	814.9 $\pm$ 140.7	394.4 $\pm$ 66.6	163.4 $\pm$ 18.7	118.9 $\pm$ 14.9
Observed Events	856	421	177	139

TABLE XI: Background estimate for events with exactly one SECVTX b-tag that passes the NN filter as a function of jet multiplicity.

Jet Multiplicity	2jet	3jet	$\geq$ 4jet
Observed Events(pretag)	14604	2362	646
Mistag	3.5 $\pm$ 0.5	2.0 $\pm$ 0.3	1.2 $\pm$ 0.2
$Wb\bar{b}$	20.3 $\pm$ 7.0	5.7 $\pm$ 1.8	1.0 $\pm$ 0.4
$Wc\bar{c}$	3.3 $\pm$ 1.1	0.4 $\pm$ 0.1	0.1 $\pm$ 0.04
Wc	-	-	-
$t\bar{t}$(6.7pb)	10.4 $\pm$ 2.3	29.5 $\pm$ 6.4	45.5 $\pm$ 9.9
Single Top	4.2 $\pm$ 0.7	1.4 $\pm$ 0.2	0.3 $\pm$ 0.1
Diboson/$Z^0 \rightarrow \tau\tau$	1.2 $\pm$ 0.3	0.3 $\pm$ 0.1	0.1 $\pm$ 0.1
non-W QCD	1.4 $\pm$ 0.3	0.9 $\pm$ 0.2	0.3 $\pm$ 0.1
Total Background	44.2 $\pm$ 8.5	40.1 $\pm$ 6.8	48.6 $\pm$ 10.0
Observed Events	39	44	65

TABLE XII: Background estimate for events with at least two SECVTX b-tagged jets as a function of jet multiplicity.

Higgs Mass (GeV/c^2)	Expected Signal Events			
	Pretag	=1 tag	=1 tag & NNtag	$\geq$ 2 tag
110	4.81±0.34	2.15 ± 0.18	1.87 ± 0.18	0.66 ± 0.13
115	3.99±0.28	1.80 ± 0.15	1.56 ± 0.15	0.54 ± 0.11
120	3.23±0.23	1.45 ± 0.12	1.26 ± 0.12	0.44 ± 0.09
130	2.05±0.15	0.93 ± 0.08	0.81 ± 0.08	0.28 ± 0.06
140	1.03±0.07	0.46 ± 0.04	0.40 ± 0.04	0.15 ± 0.03
150	0.40±0.03	0.18 ± 0.02	0.16 ± 0.02	0.06 ± 0.01

TABLE XIII: Expected number $WH \to \ell\nu b\bar{b}$ signal events in W+2jets event for various b-tagging options, where "tag" and "NNtag" stand for SECVTX b-tagging and Neural Network b-tagging, respectively.

source	uncertainty (%)		
	= 1 Tag	= 1 Tag & NNtag	$\geq$ 2 Tag
Lepton ID	~2%	~2%	~2%
Trigger	<1%	<1%	<1%
ISR	1.5%	1.8%	4.3%
FSR	2.8%	3.2%	8.6%
PDF	1.6%	1.7%	2.0%
JES	2.3%	2.3%	3.0%
b-tagging	3.8%	5.3%	16%
Total	5.8%	7.2%	19.1%

TABLE XIV: Systematic uncertainties for various b-tagging requirements. "Tag" and "NNtag" represent tight SECVTX and Neural Network b-tagging respectively.

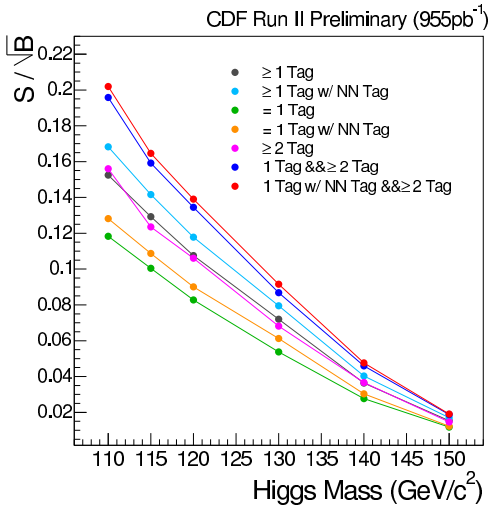

FIG. 13: Comparison of significance obtained from various b-tagging strategies. "Tag" and "NN Tag" represent SECVTX and Neural Network b-tagging respectively. The symbol "&&" means a combined use of the two strategies.

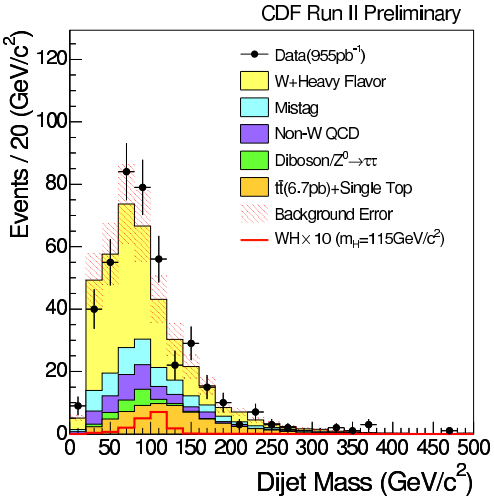

FIG. 14: Dijet mass distribution in W+2jets events including exactly one SECVTX b-tagged jet that passes Neural Network b-tagging filter. Each contribution of the background sources are written in histogram, while the hatched box on the background histogram represents the background uncertainty. The $WH \to \ell\nu b\bar{b}$ signal is scaled by a factor of 10 and drawn in solid (red) line.

where n_i, μ_i and $N_{\rm bin}$ stand for the number of observed data in i-th bin, the expectation in i-th bin and the total number of bins. The Higgs production hypothesis is constructed by setting μ_i as:

$$\mu_i = s_i + b_i, \tag{17}$$

where s_i and b_i are the number of signal and expected background events in i-th bin respectively. In this hypothesis, s_i is a free variable to be extracted from data. This quantity s_i can also be written as a product:

$$s_i = \sigma(p\bar{p} \to W^{\pm}H) \cdot Br(H \to b\bar{b}) \cdot \epsilon_{WH \to \ell\nu b\bar{b}} \cdot \int \mathcal{L}dt \cdot f_i^{(WH \to \ell\nu b\bar{b})}, \tag{18}$$

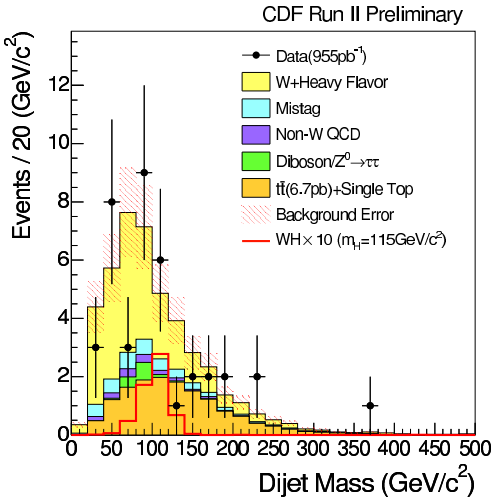

FIG. 15: Dijet mass distribution in W+2jets events including at least two SECVTX b-tagged jets. The contributions of the individual background sources are shown, while the hatched box on the background histogram is the total background uncertainty. The expected $WH \to \ell\nu b\bar{b}$ signal rate is scaled by a factor of 10 and drawn in solid (red) line.

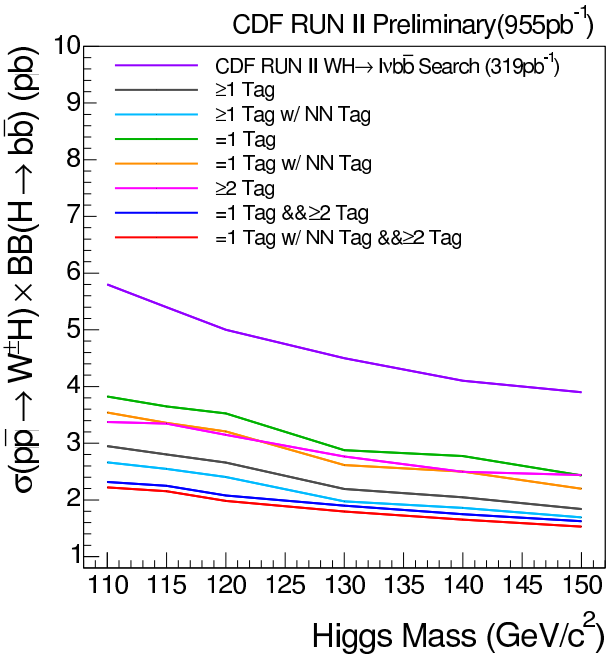

FIG. 16: Expected upper limits on Higgs boson production cross section times branching ratio $WH \to \ell\nu b\bar{b}$ obtained with various b-tagging strategies. "Tag" and "NN Tag" refer to SECVTX and Neural Network b-tagging, respectively The purple line is the expected 95% C.L. upper limit obtained by the previous analysis with 319 pb^{-1}.

where $f_i^{(WH\to\ell\nu b\bar{b})}$ is a signal fraction in i-th bin. $\epsilon_{WH\to\ell\nu b\bar{b}}$ and $\int \mathcal{L}dt$ are obtained in **Secs.VI** and **IV** respectively. In this case, $\sigma(p\bar{p} \to W^{\pm}H) \cdot Br(H \to b\bar{b})$ is the variable to be extracted from data, and the Higgs production hypothesis is interpreted as "the Standard Model Higgs boson exists with a certain value of $\sigma(p\bar{p} \to W^{\pm}H) \cdot Br(H \to b\bar{b})$ at specific confidence interval.". Then the alternative (null) hypothesis is interpreted as "the Standard Model Higgs bosons production is not larger than a certain value of $\sigma(p\bar{p} \to W^{\pm}H) \cdot Br(H \to b\bar{b})$ at specific confidence level(C.L.)." An upper limit on the Higss boson production cross section times branching ratio is derived by comparing these two hypotheses. The extraction of the parameter of $\sigma(p\bar{p} \to W^{\pm}H) \cdot Br(H \to b\bar{b})$ is performed by using maximum likelihood method with a likelihood defined by:

$$L = \prod_{i=1}^{N_{\rm bin}} P_i(n_i, \mu_i) = \prod_{i=1}^{N_{\rm bin}} \frac{\mu_i^{n_i} e^{-\mu_i}}{n_i!}. \qquad (19)$$

The background prediction b_i includes contributions from the various background sources described in Section **??**:

$$b_i = N^{(TOP)} f_i^{(TOP)} + N^{(QCD)} f_i^{(QCD)}, \qquad (20)$$

where $f_i^{(TOP)}$ and $f_i^{(QCD)}$ are the background fractions of each background sources in i-th bin. Both the number of signal events and the expected background have systematic uncertainties. Let the systematic uncertainties convoluted with the binned likelihood be

$$L(\sigma \cdot Br) = \int_{N_{QCD}} \int_{N_{TOP}} \int_{N_{WH}} \prod_{i=1}^{N_{\rm bin}} \frac{\mu_i^{n_i} e^{-\mu_i}}{n_i} \times G(N_{QCD}, \sigma_{QCD}) G(N_{TOP}, \sigma_{TOP}) G(N_{WH}, \sigma_{WH}) dN_{QCD} d$$

An upper limit on $\sigma \cdot Br$ is obtained by examining one side of the likelihood distribution. Let β be the cumulative probability of a variable α defined as:

$$\beta = \frac{\int_0^{\alpha_\beta} L(\alpha) d\alpha}{\int_0^{\infty} L(\alpha) d\alpha}, \qquad (22)$$

where α_β is the upper limit of the variable α at confidence level of β. In this analysis, β is set at 0.95 and the upper limit on $\sigma(p\bar{p} \to WH) \cdot Br(H \to b\bar{b})$ is calculated at 95% C.L.

Before looking at the upper limit obtained from data, pseudo-experiment are performed to calculated an expected limit in the absence of Higgs boson production. Pseudo-data are generated by fluctuating the individual background estimates within total uncertainties. The expected limit is derived from the pseudo-data using Eqs.21 and 22.

The expected limits from various b-tagging strategies are shown in Fig.16. The upper limit obtained by com-

bining likelihoods from events with exactly one SECVTX b-tagged jet passing Neural Network b-tagging criteria and events with at least two SECVTX b-tagged jets criteria is computed as:

$$L(\sigma{\cdot}Br) = L(\sigma{\cdot}Br\,|1 \text{ Tag w/ NN Tag}){\times}L(\sigma{\cdot}Br\,|\geq 2 \text{ Tag}), \quad (23)$$

where the correlations between "=1 Tag w/ NN Tag" and "$\geq$ 2 Tag" events are taken into account. The systematic uncertainty up to the pretag acceptance, luminosity uncertainty, and uncertainty of b-tagging scale factor are considered to be 100% correlated between the two selection types. In accordance with Fig.16, "=1 tag w/ NNtag" combined with "$\geq$2 Tag" gives the best expected limit, as expected from the sensitivity study (see Fig.13).

Finally we set an upper limit on $\sigma(p\bar{p} \rightarrow WH) \cdot Br(H \rightarrow b\bar{b})$ with the combined likelihood The likelihood distributions before and after the combination are shown in Fig.?? for a Higgs boson mass of 115 GeV/c^2. The observed limit as a function of the Higgs boson mass is shown in Fig.17 and Table XV together with the expected limit. The observed limit around 115 GeV/c^{2}is slightly higher than the expectation. To see if the obtained limit is reasonable or not, the results of pseudo experiments and the observed limit for each Higgs boson mass point are show in Fig.18. The limit in the low mass region is somewhat worse than expected, but this also can be understood as a statistical fluctuation in dijet mass distributions (see Fig.14) around $m_H = 115$ GeV/c^2.

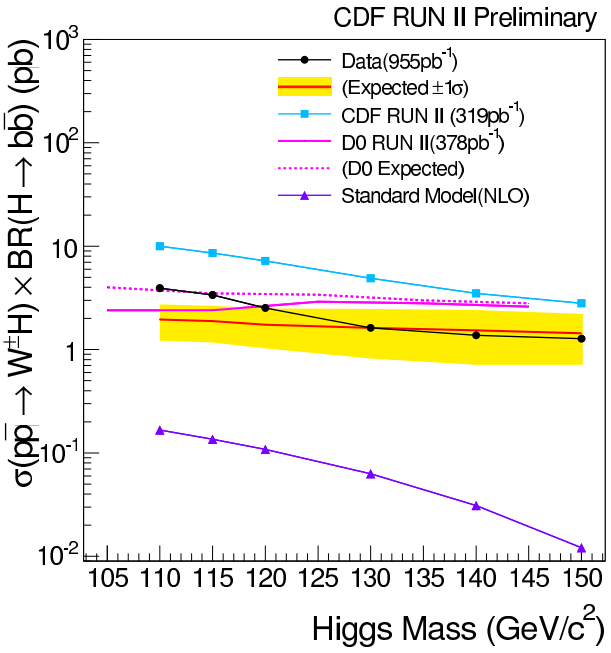

FIG. 17: 95% confidence level upper limit on $\sigma(p\bar{p} \rightarrow WH) \cdot Br(H \rightarrow b\bar{b})$ with an integrated luminosity of 955 pb^{-1} obtained from the combined likelihood between events with exactly one SECVTX b-tag passing Neural Network b-tagging and events with at least two SECVTX b-tagged jets.

Higgs Mass	Upper Limit(pb)	
GeV/c^2	Observed	Expected
110	4.9	2.2±0.8
115	3.4	2.2±0.8
120	2.5	2.0±0.7
130	1.6	1.8±0.7
140	1.4	1.7±0.6
150	1.3	1.5±0.6

TABLE XV: Observed and expected upper limit on $\sigma(p\bar{p} \rightarrow WH) \cdot Br(H \rightarrow b\bar{b})$ at 95 % C.L.

IX. CONCLUSIONS

We have presented a search for the Standard Model Higgs boson in the $\ell\nu b\ barb$ final state expected from WH production. The event selection includes a novel neural network b-tag filter to reduce the background contributions from light flavor and charm quark jets. This improvement, along with a total dataset corresponding to 1 fb^1 allows us to improve the upper limit on Higgs boson production. We set a 95% confidence level upper limit on the production cross section times branching ratio of 3.9 to 1.3 pb for Higgs boson mass 110 to 150GeV/c^2.

Acknowledgments

We thank the Fermilab staff and the technical staffs of the participating institutions for their vital contributions. This work was supported by the U.S. Department of Energy and National Science Foundation; the Italian Istituto Nazionale di Fisica Nucleare; the Ministry of Education, Culture, Sports, Science and Technology of Japan; the Natural Sciences and Engineering Research Council of Canada; the National Science Council of the Republic of China; the Swiss National Science Foundation; the A.P. Sloan Foundation; the Bundesministerium für Bildung und Forschung, Germany; the Korean Science and Engineering Foundation and the Korean Research Foundation; the Particle Physics and Astronomy Research Council and the Royal Society, UK; the Institut National de Physique Nucleaire et Physique des Particules/CNRS; the Russian Foundation for Basic Research; the Comisión Interministerial de Ciencia y Tecnología, Spain; the European Community's Human Potential Programme under contract HPRN-CT-2002-00292; and the Academy of Finland.

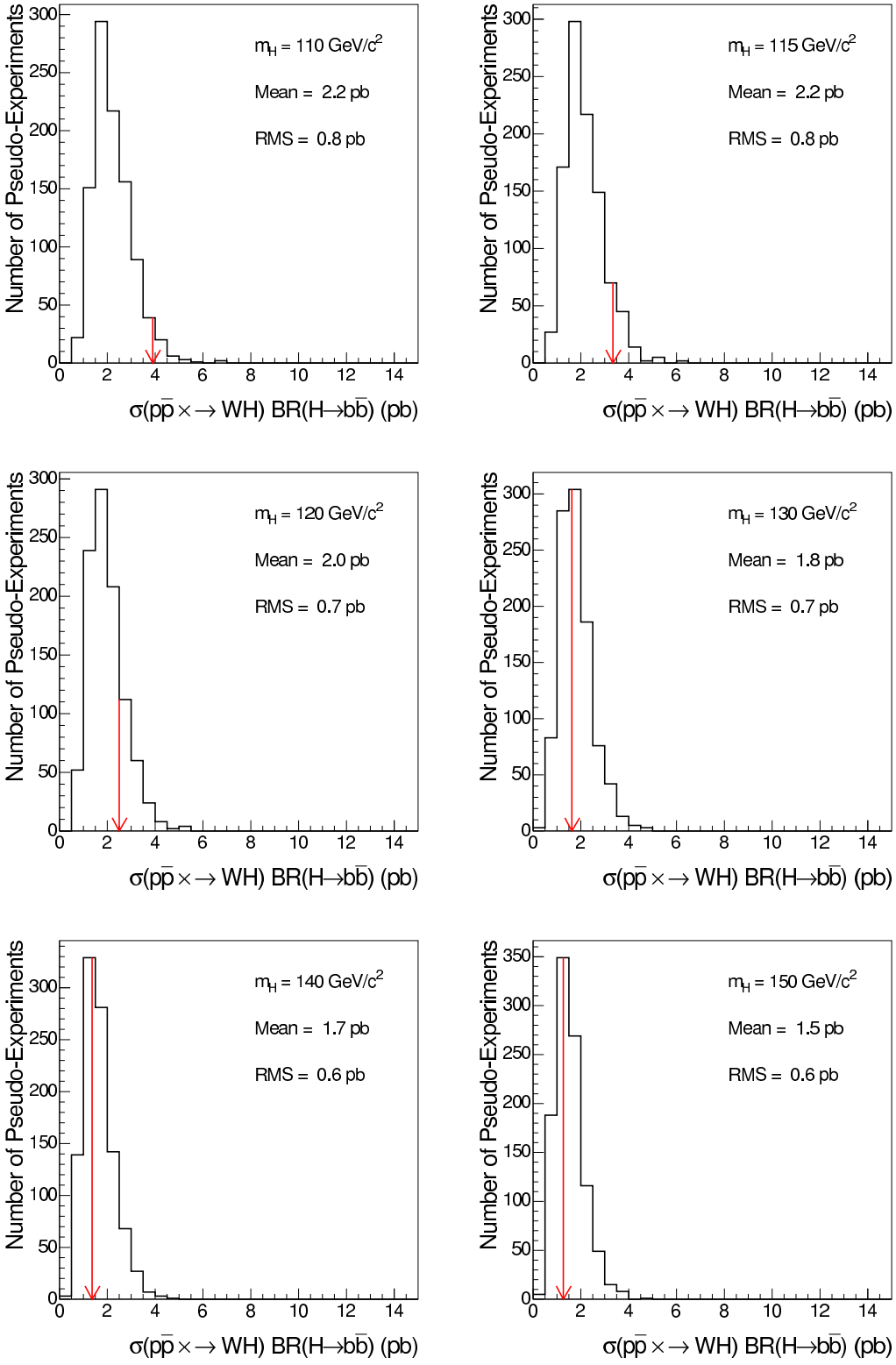

FIG. 18: The result of pseudo-experiments obtained from the combined likelihood. Red arrows are pointing the observed limits.

[1] ALEPH and DELPHI and L3 and OPAL Collaboration and the LEP Working Group for Higgs Boson Searches, Phys. Lett. B **565** (2003).

[2] LEP Electroweak Working Group, `http://lepewwg.web.cern.ch/LEPEWWG/` (????).

[3] J. Conway, `http://www.physics.ucdavis.edu/~conway/research/higgs.html` (????).

[4] A. Djouadi, J. Kalinowski, and M. Spira, Comp. Phys. Comm. **108** (1998).

[5] A. Abulencia et al., Phys. Rev. Lett. **96** (2006).

[6] W. Abazov et al., Phys. Rev. Lett. **94** (2005).

[7] D. Acosta et al., Phys. Rev. D **72** (2005).

[8] L. Cerrito and A. Taffard, CDF-6305 (2003).

[9] A. Abulencia et al., arXiv:hep-ex/0607035, submitted to Phys. Rev. **D** (2006).

[10] D. Acosta et al., CDF-6315 (2003).

[11] C. Neu et al., CDF-7578 (2005).

[12] StatSoft, Inc., Neural Networks `http://www.statsoft.com/textbook/stneunet.html` (1984-2003).

[13] C. Peterson, T. Rögnavaldsson, and L. Lönnbald, Comp. Phys. Comm. **81** (1994).

[14] H. Bachacou, J. Nielsen, and W. Yao, CDF-6569 v1.0 (2004).

[15] H. Bachacou, J. Nielsen, and W. Yao, CDF-6569 v2.0 (2004).

[16] J. Guimaraes and C. S. Rappoccio, CDF-7326 (2006).

[17] D. Sherman, S. Rappoccio, and J. G. da Costa, CDF-7585 (2005).

[18] S. Budd, T. Junk, and C. Neu, CDF-8072 (2006).

[19] H. Bachacou et al., CDF-7007 (2004).

[20] M. L. Mangano et al., arXiv:hep-ph/0206293 (2003).

[21] G. Corcella et al., arXiv:hep-ph/0201201 (2002).

[22] J. M. Campbell and R. K. Ellis, Phys. Rev. D **65** (2002).

[23] D. Acosta et al., Phys. Rev. Lett. **94** (2005).

[24] M. Cacciari et al., arXiv:hep-ph/0303085 (2005).

[25] B. W. H. Laenen et al., Phys. Rev. D **66** (2002).

[26] T. Sjöstrand and L. Lönnbald, arXiv:hep-ph/0108264 (2001).

[27] C. Hill, J. Incandela, and C. Mills, CDF-7309 (2005).

[28] V. Martin, CDF-7031 (2005).

[29] U. Grundler, A. Taffard, and X. Zhang, CDF-7956 (2005).

[30] U. Grundler, A. Taffard, and X. Zhang, CDF-7262 (2006).

[31] Y. Ishizawa and J. Nielsen, CDF-7401 (2005).

[32] V. Boisvert, CDF-7939 (2005).

[33] In this paper, lepton(ℓ) denotes electron($e^{\pm}$) or muon($\mu^{\pm}$).

[34] The following track paraemters are used to determined the quality of a track: transverse momentum, number of silicon hits attached, quality of those hits, and $\chi^2/N_{\rm DOF}$.

[35] Some care must be taken since the CDF origin is taken to be the center of the COT which is not the origin of the SVX. (the SVX center is shifted approximately (-1mm,+1mm) with respect to the COT origin)

[36] The background estimate shown in section V implies that about 50% of the SECVTX tagged jets are from falsely tagged light flavor or gluon jets and c-jets.

[37] A small but purified b-jet sample is obtained by requiring a soft lepton in the jet.

[38] Track segment reconstructed by 4 layer structure in CMU, CMP and CMX is called as "stub".

[39] Object that passes all of the lepton identification criteria except for isolation requirement.